

CERN-EP-2023-131
07 July 2023

Measurement of inclusive charged-particle jet production in pp and p–Pb collisions at $\sqrt{s_{\text{NN}}} = 5.02$ TeV

ALICE Collaboration*

Abstract

Measurements of inclusive charged-particle jet production in pp and p–Pb collisions at center-of-mass energy per nucleon–nucleon collision $\sqrt{s_{\text{NN}}} = 5.02$ TeV and the corresponding nuclear modification factor $R_{\text{pPb}}^{\text{ch jet}}$ are presented, using data collected with the ALICE detector at the LHC. Jets are reconstructed in the central rapidity region $|\eta_{\text{jet}}| < 0.5$ from charged particles using the anti- k_T algorithm with resolution parameters $R = 0.2, 0.3,$ and 0.4 . The p_T -differential inclusive production cross section of charged-particle jets, as well as the corresponding cross section ratios, are reported for pp and p–Pb collisions in the transverse momentum range $10 < p_{T,\text{jet}}^{\text{ch}} < 140$ GeV/ c and $10 < p_{T,\text{jet}}^{\text{ch}} < 160$ GeV/ c , respectively, together with the nuclear modification factor $R_{\text{pPb}}^{\text{ch jet}}$ in the range $10 < p_{T,\text{jet}}^{\text{ch}} < 140$ GeV/ c . The analysis extends the p_T range of the previously-reported charged-particle jet measurements by the ALICE Collaboration. The nuclear modification factor is found to be consistent with one and independent of the jet resolution parameter with the improved precision of this study, indicating that the possible influence of cold nuclear matter effects on the production cross section of charged-particle jets in p–Pb collisions at $\sqrt{s_{\text{NN}}} = 5.02$ TeV is smaller than the current precision. The obtained results are in agreement with other minimum bias jet measurements available for RHIC and LHC energies, and are well reproduced by the NLO perturbative QCD POWHEG calculations with parton shower provided by PYTHIA8 as well as by JETSCAPE simulations.

arXiv:2307.10860v2 [nucl-ex] 7 Jun 2024

1 Introduction

In high-energy hadronic collisions, scattering processes at very large momentum transfer Q^2 between quarks and gluons of the colliding nucleons produce parton showers, which subsequently fragment into collimated sprays of hadrons called jets. Studies of jet production in proton–proton (pp) collisions allow one to test the fixed-order perturbative quantum chromodynamics (pQCD) calculations of the jet production in the TeV domain and tune the higher order effects in QCD-based Monte Carlo (MC) event generators [1–4]. Furthermore, such studies, especially at low p_T , constrain the non-perturbative contributions, such as the hadronization and underlying event effects, to the inclusive jet cross section. In addition, measurements in pp collisions also provide the baseline for similar measurements in proton–nucleus (pA) and nucleus–nucleus (AA) collisions. Comparing the jet production between pp and pA collisions allows for an assessment of the effects related to the presence of bound nucleons in the colliding system, denoted as cold nuclear matter (CNM) effects at the initial state of the collisions, which can be described by partonic rescattering [5] and by modification of parton distribution functions (PDFs) [6]. The study of these CNM effects is interesting in its own right since it is necessary to decouple the CNM effects from those related to the creation of the quark–gluon plasma (QGP), which is a hot and dense color-deconfined QCD matter created in AA collisions [7, 8].

The production of the QGP in AA collisions is confirmed by many observations (see in [9] and the references therein). One of the QGP signatures is the so-called jet quenching phenomenon. It is manifested by the suppression of high- p_T hadron and jet yields with respect to those in pp collisions [10, 11]. One microscopic picture of this phenomenon assumes that, while traversing through the QGP, the initial highly-energetic parton loses energy via medium-induced gluon radiations and elastic scatterings with constituents of the hot and dense medium. A convenient observable to quantify these jet quenching effects is the nuclear modification factor, defined as the ratio of the jet (or final-state hadron) yield produced in AA or pA collisions to that in pp collisions, scaled by the average number of nucleon–nucleon collisions $\langle N_{\text{coll}} \rangle$ [12]. A deviation from one of this ratio at high p_T indicates the presence of nuclear effects.

Initially, the pA system was thought to be too small to create a QGP. However, recent measurements show evidence of collective behavior in high-multiplicity pp and p–Pb collisions at the LHC [13–16] and in light nucleus–Au collisions at RHIC [17, 18]. By contrast, jet quenching phenomena have not yet been seen in small collision systems. The question of possible QGP formation in small collision systems remains open and calls for further, more precise jet quenching searches. The production of charged-particle jets and the corresponding nuclear modification factor $R_{\text{pPb}}^{\text{ch jet}}$ in p–Pb collisions at center-of-mass energy per nucleon–nucleon collision $\sqrt{s_{\text{NN}}} = 5.02$ TeV were previously reported by the ALICE Collaboration based on Run 1 data [19]. The scaled p_T -differential charged-particle jet production cross section from pp collisions at $\sqrt{s} = 7$ TeV was adopted for calculating the $R_{\text{pPb}}^{\text{ch jet}}$ in this study, and results show that the $R_{\text{pPb}}^{\text{ch jet}}$ is consistent with one within uncertainties. The measurement of full jet production in p–Pb collisions at $\sqrt{s_{\text{NN}}} = 5.02$ TeV has been presented by the ATLAS [20] and CMS Collaborations [21] at the LHC, and in d–Au collisions at $\sqrt{s_{\text{NN}}} = 200$ GeV by the PHENIX Collaboration [22] at RHIC.

In this article, we revisit previous ALICE analyses by measuring the charged-particle jet production in the larger Run 2 datasets of pp and p–Pb collisions at $\sqrt{s_{\text{NN}}} = 5.02$ TeV, exploiting the excellent tracking capabilities of ALICE [23, 24]. These large data samples enable higher precision measurement of the charged-particle jet production over a broader $p_{T,\text{jet}}^{\text{ch}}$ interval compared to the previous one [19], extending $p_{T,\text{jet}}^{\text{ch}}$ down to 10 GeV/ c and up to 140 GeV/ c . Furthermore, in contrast to the results from Run 1, the reported $R_{\text{pPb}}^{\text{ch jet}}$ from Run 2 utilizes a pp reference measured at the same collision energy. Therefore, when constructing the nuclear modification factor, there is no need to rely on an interpolation between collision energies; instead, a more direct comparison can be made at the same $\sqrt{s_{\text{NN}}}$. This reduces the normalization uncertainty by a factor of about 2.7 as compared to the previously published

results. Data from Pb–Pb collisions are also available at the same energy [25, 26] and thus the results from this p–Pb analysis can provide a baseline for the Pb–Pb data. These measurements can also be used to constrain the nuclear-modified parton distribution functions (nPDFs) [27–30] and the strong coupling constant α_s [31].

This article reports the measurement of charged-particle jet production both in pp and p–Pb collisions at $\sqrt{s_{\text{NN}}} = 5.02$ TeV and the corresponding nuclear modification factor for jet resolution parameters $R = 0.2, 0.3,$ and 0.4 . The inclusive jet cross section is used to evaluate ratios of jet yields obtained for different resolution parameters. These ratios provide insight into the interplay between perturbative and non-perturbative effects on jet transverse momentum scales [1, 32–34].

The paper is organized as follows. Section 2 describes the ALICE detector and the dataset. Jet reconstruction approach, correction for detector and acceptance efficiency, and systematic uncertainty assessment are discussed in Section 3. Section 4 presents the results and compares them to theoretical predictions and other experimental measurements. The conclusion is given in Section 5.

2 Experimental setup and datasets

The ALICE detector is a general-purpose heavy-ion experiment at the LHC [24, 35]. The pp dataset used in this analysis was collected in 2017 at $\sqrt{s} = 5.02$ TeV, while the p–Pb dataset was collected in 2016 at $\sqrt{s_{\text{NN}}} = 5.02$ TeV, during the LHC Run 2. The analyzed data samples were collected with a minimum bias (MB) trigger and consist of 968×10^6 MB events for pp collisions, corresponding to an integrated luminosity $L_{\text{pp}} = 18.9 \pm 0.4 \text{ nb}^{-1}$ [36], and 624×10^6 MB events for p–Pb collisions, corresponding to $L_{\text{pPb}} = 298 \pm 11 \text{ } \mu\text{b}^{-1}$ [37]. In p–Pb collisions, a rapidity shift $\Delta y = 0.465$ is needed in the direction of the proton beam to transform from the ALICE laboratory frame to the nucleon–nucleon center-of-mass frame due to the asymmetry of the colliding beam energies; protons at 4 TeV energy are collided into fully stripped $^{208}_{82}\text{Pb}$ ions at 1.58 TeV per nucleon energy [38].

Events were triggered using the V0 detector [39], which consists of two scintillator arrays located at forward and backward rapidity. It covers the pseudorapidity regions $-3.7 < \eta < -1.7$ (V0C) and $2.8 < \eta < 5.1$ (V0A). To select the MB trigger, coincident signals are required in both the V0A and V0C detectors. Beam-induced background events, such as beam–gas interactions or out-of-bunch pileup within the V0 detector readout time, are rejected offline by using the timing information from the V0 detectors and the number of reconstructed points and track segments in the Silicon Pixel Detector (SPD), which are expected to be uncorrelated for background events. The SPD equips the two innermost layers of the Inner Tracking System (ITS), a silicon tracker with six layers, and covers the pseudorapidity interval $|\eta| < 1.4$ around midrapidity. In-bunch pileup events, where multiple interactions occur in the same bunch crossing, are rejected by requiring that only a single primary vertex is reconstructed with the SPD in the event [24]. For the data samples considered in this paper, pileup events amount to less than 1% of the event sample both in pp and p–Pb collisions [40]. Accepted events are required to have the reconstructed primary vertex position along the beam axis within 10 cm from the center of the detector [24].

Charged-particle jets are reconstructed using tracks of primary-charged-particle candidates produced in the collision. Primary charged particles are defined as all particles with a mean proper lifetime $\tau > 1 \text{ cm}/c$ which are either produced directly in the interaction or from decays of particles with a mean proper lifetime $\tau < 1 \text{ cm}/c$. This excludes particles produced in interactions with the detector material and products of weak decays [41]. The charged-particle trajectories are reconstructed using information from the ITS [23] and the Time Projection Chamber (TPC) [42]. These detectors are located inside a large solenoidal magnet that provides a uniform magnetic field of $B = 0.5 \text{ T}$. Tracks were selected with transverse momenta $p_{\text{T,track}} > 0.15 \text{ GeV}/c$ and in a pseudorapidity range $|\eta| < 0.9$ over the full azimuth $0 < \phi < 2\pi$.

In order to achieve a uniform azimuthal angle distribution and the high-quality momentum resolution required for jet reconstruction, the charged track selection utilized a hybrid selection technique that compensates for local inefficiencies in the SPD. Two distinct classes of tracks are combined in the hybrid approach [43]. The first class consists of tracks that have at least one hit in the SPD. The second class contains tracks without hits in the SPD, in which case the primary interaction vertex is used to constrain the trajectory in the track fit to improve the determination of their transverse momentum. The charged track momentum resolution $\sigma(p_T)/p_T$ is estimated using the covariance matrix of the track fit [24] and is approximately 0.8% at $p_{T,\text{track}} = 1 \text{ GeV}/c$ and 4% at $p_{T,\text{track}} = 50 \text{ GeV}/c$.

Data corrections on instrumental effects were based on Monte Carlo (MC) simulations, which included a detailed description of the detector geometry and response, using the GEANT3 package [44]. The simulations were performed using the PYTHIA8 event generator [45] with the Monash 2013 tune [46] for pp collisions and the PYTHIA6 [47] with the Perugia 2011 tune [48] for p–Pb collisions. The simulated data were analyzed in the same way as the real data.

3 Data analysis

3.1 Jet reconstruction

The strategy for the jet reconstruction closely followed the procedures used by the ALICE Collaboration in the Run 1 analysis, including the background density estimation [19]. Jet finding was performed using the FastJet 3.2.1 [49] package. Signal jets were reconstructed from charged-particle tracks using the anti- k_T sequential clustering algorithm [50] with resolution parameters $R = 0.2, 0.3, \text{ and } 0.4$. The four-momenta of the jet constituents were combined using the boost-invariant p_T recombination scheme, treating the jet constituents as massless. To ensure that jets were well contained in the TPC acceptance, the pseudorapidity coverage of the reconstructed jets was constrained to $|\eta_{\text{jet}}| < 0.5$ for all jet resolution parameters. The area of the jet was required to be $A_{\text{jet}} > 0.6\pi R^2$ to suppress the contribution from pure background jet clusters [26]. Jets which contained tracks with p_T larger than $100 \text{ GeV}/c$ were rejected, in order to suppress contamination by fake tracks and ensure good momentum resolution. This selection rejects less than 1% of jets in the considered kinematic region, and the impact on the raw jet spectrum is minor.

Reconstructed jets from the hard process are always accompanied by soft background that does not originate from the hard process, known as the underlying event. The transverse momentum of selected signal jets in p–Pb collisions was subsequently corrected for the average underlying event contribution [51] according to the formula

$$p_{T,\text{jet}}^{\text{ch}} = p_{T,\text{jet}}^{\text{ch,raw}} - \rho_{\text{ch}} \times A_{\text{jet}}, \quad (1)$$

where the transverse momentum density ρ_{ch} of particles produced by the underlying event in p–Pb collisions was estimated on an event-by-event basis using the so-called improved CMS method [52]

$$\rho_{\text{ch}} = \text{median} \left\{ \frac{p_{T,\text{jet}}^{k_T}}{A_{\text{jet}}^{k_T}} \right\} \times C. \quad (2)$$

Here $A_{\text{jet}}^{k_T}$ and $p_{T,\text{jet}}^{k_T}$ are the area and the transverse momentum of the jet clusters found using the k_T algorithm. The k_T jets had the same resolution parameter as the anti- k_T jets, and the pseudorapidity range of the reconstructed k_T jets spanned $|\eta_{\text{jet}}| < 0.9$. The jet active area [53] was estimated by distributing ghost particles into the η – ϕ acceptance. The ghost particle density is 200 per unit area and corresponds to 0.005 area per ghost particle. The two highest- p_T jets in the event were excluded from the estimation of the background in order to suppress impact of physical jets on ρ_{ch} [54]. The scaling factor C is used to account for regions without particles. It is defined as

$$C = \frac{\sum_j A_j}{A_{\text{acc}}}. \quad (3)$$

Here A_j is the area of each k_T jet with at least one real track (i.e. excluding ghosts), and A_{acc} is the area of charged-particle acceptance. In pp collisions, the underlying event constitutes approximately $p_T = 1 \text{ GeV}/c$ per jet, and was not subtracted from the raw jet spectrum [55].

3.2 Corrections

The measured jet spectrum is distorted predominantly due to the finite detector resolution and local background fluctuations with respect to the mean underlying event density. A correction procedure known as unfolding was used to correct for these effects [56, 57]. The response matrices for these two effects are determined separately and combined by making a product of the two [58].

The response matrix describing jet momentum smearing due to instrumental effects was determined from the PYTHIA MC simulation. Detector-level jets were reconstructed by transporting the generated particles through a full simulation of the ALICE detector using the GEANT3 transport model [59]. These jets were geometrically matched to the corresponding particle-level jets on a jet-by-jet basis by requiring that the angular distance $\Delta R = \sqrt{(\Delta\eta)^2 + (\Delta\phi)^2} < 0.6R$, where $\Delta\eta$ and $\Delta\phi$ are the differences in pseudorapidity and azimuthal angle between the detector-level and particle-level jets. The particle-level jets were reconstructed without imposing any selection on the constituents. Consequently, during the unfolding process, the reconstructed jets are corrected to a constituent-charged-particle momentum of 0 GeV/c.

The probability of a particle-level jet not matching any detector-level jet is considered as the jet reconstruction efficiency, is applied to correct the unfolded jet spectrum. Its value is about 80% at jet $p_T \approx 10 \text{ GeV}/c$ and increases to 99% for jets with $p_T > 30 \text{ GeV}/c$ in the considered kinematic region. Additionally, the probability that a detector-level jet is falsely matched to a non-corresponding particle-level jet is called the jet reconstruction purity. The jet reconstruction purity is found to be above 99% in the measured kinematic range. Hence, the raw jet spectrum was not corrected for the reconstruction purity.

The performance of the jet reconstruction was assessed using the MC simulation. Two variables are evaluated: the shift of the mean jet energy scale (JES) $\Delta_{\text{JES}} = \left\langle (p_{T,\text{jet}}^{\text{ch det}} - p_{T,\text{jet}}^{\text{ch truth}}) / p_{T,\text{jet}}^{\text{ch truth}} \right\rangle$ and the jet energy resolution $\text{JER} = \sigma(p_{T,\text{jet}}^{\text{ch det}}) / p_{T,\text{jet}}^{\text{ch truth}}$, where $p_{T,\text{jet}}^{\text{ch det}}$ and $p_{T,\text{jet}}^{\text{ch truth}}$ are the transverse momenta of the measured jet and the corresponding truth jet, and $\sigma(p_{T,\text{jet}}^{\text{ch det}})$ denotes the width of the $p_{T,\text{jet}}^{\text{ch det}} - p_{T,\text{jet}}^{\text{ch truth}}$ distribution as a function of $p_{T,\text{jet}}^{\text{ch truth}}$. The Δ_{JES} distribution is asymmetric and has a long negative tail due to the reconstruction inefficiency and a sharp peak centered around $p_{T,\text{jet}}^{\text{ch truth}} = p_{T,\text{jet}}^{\text{ch det}}$. The most probable scenario is that the measured $p_{T,\text{jet}}^{\text{ch}}$ is close to the jet p_T at particle level. The Δ_{JES} distribution has a mean value of -15% (-20%) and -27% (-30%) for the $p_{T,\text{jet}}^{\text{ch truth}}$ interval $20 < p_{T,\text{jet}}^{\text{ch truth}} < 30 \text{ GeV}/c$ and $100 < p_{T,\text{jet}}^{\text{ch truth}} < 120 \text{ GeV}/c$, respectively, for pp (p–Pb) collisions. The value of the JER varies from 23% (20%) to 27% (38%) in pp (p–Pb) collisions at $p_{T,\text{jet}}^{\text{ch truth}} = 20 \text{ GeV}/c$ and $p_{T,\text{jet}}^{\text{ch truth}} = 150 \text{ GeV}/c$, respectively. Both Δ_{JES} and JER exhibit a weak R dependence.

The response matrix which accounts for the smearing due to local background fluctuations, was obtained with the random cone (RC) method [60]. Cones with a resolution parameter R_{cone} equal to that of the jet were placed randomly in the $\eta - \phi$ space in each event, within the ITS and TPC acceptance. The background fluctuations were evaluated by comparing the sum of the p_T of tracks inside the cone, p_T^{RC} , with the expected average contribution due to the underlying event as follows:

$$\delta p_T^{\text{RC}} = p_T^{\text{RC}} - \rho_{\text{ch}} \pi R_{\text{cone}}^2. \quad (4)$$

In this study, two definitions for the random cone were considered. First, the random cones were required not to overlap with the leading and subleading jets in an event. Second, the cones were placed in a perpendicular direction to the leading jet in an event. These two approaches yield a consistent result and their difference was considered as a source of systematic uncertainty. The nominal result used

the δp_T^{RC} matrix obtained by the first approach. The corresponding δp_T^{RC} distribution has a width of $\sigma^{\text{RC}} = 2.01$ GeV/ c for $R = 0.2$, 3.01 GeV/ c for $R = 0.3$, and 4.01 GeV/ c for $R = 0.4$. The response matrix for the local background fluctuations was constructed row-by-row by taking the δp_T^{RC} distribution and shifting it along the $p_{\text{T,jet}}^{\text{ch det}}$ axis by the amount $p_{\text{T,jet}}^{\text{ch truth}}$ corresponding to each row [58]. In pp collisions, no correction for the background fluctuations was applied, and the raw spectrum was corrected for the instrumental effects only.

In our case the use of an unregularized unfolding method led to a non-physically behaving solution, which wildly oscillated due to statistical fluctuations of the measured spectrum. To suppress these fluctuations, unfolding algorithms which impose a smoothness criterion were used in this analysis. The regularization procedure introduces additional systematic uncertainties on the unfolded spectrum, as discussed in Sec. 3.3.2. The singular value decomposition (SVD-) based method [61] was used to perform the unfolding correction for the primary analysis. The optimum regularization parameter, k_{reg} , was chosen such that it corresponds to the point at which statistically significant components of the d -vector distribution change to noise. The values of $k_{\text{reg}} = 4$ and 6 are adopted for pp and p–Pb collisions, respectively. The unfolding was also performed using the iterative Bayesian method [62]. For the regularization of the Bayesian unfolding, convergence was determined by the stability of the unfolded solution to successive iterations, while minimizing the statistical uncertainties [63]. The convergence was achieved after the second iteration for both pp and p–Pb collisions. These unfolding algorithms are implemented in the RooUnfold framework [64]. The difference between the two unfolding methods was assigned as a source of systematic uncertainty. Input to the unfolding was the raw jet spectrum measured in the range $10 < p_{\text{T,jet}}^{\text{ch}} < 140$ GeV/ c for pp collisions and $10 < p_{\text{T,jet}}^{\text{ch}} < 160$ GeV/ c for p–Pb collisions. The fraction of particle-level jets that are reconstructed outside the measured range, referred as the kinematic efficiency, is applied to the unfolded spectrum in addition to the jet reconstruction efficiency correction. The kinematic efficiency is above 80% in the measured range. The unfolding correction required a prior spectrum as the starting point of the algorithm. In this analysis, by default the prior spectrum was defined by the particle-level distribution generated using the PYTHIA simulation. The unfolding correction of the raw jet spectrum ranges from 30% to 60% across the analyzed p_{T} range.

The robustness of the unfolding procedure and the mathematical validity of the unfolded solution were established through refolding and closure tests as done in the previous ALICE jet measurements [63]. In the refolding test, the unfolded spectrum was multiplied by the response matrix and the resulting distribution was compared to the raw jet spectrum. The closure test involved the use of two statistically independent MC samples. The first sample was utilized to construct the response matrix and provide the prior distribution. The second one served to generate pseudo-data, which were obtained by resampling the central values using Poissonian smearing. The pseudo-data was then unfolded in the same way as the real data and compared to the particle-level distribution. Within statistical uncertainties, the solutions from both tests were able to recover the input distribution.

Statistical uncertainties of the unfolded solutions were evaluated based on pseudo-random experiments. In this approach, the bin contents of the input measured spectrum were smeared according to given statistical uncertainties obtaining an ensemble of randomized spectra. The unfolding was then applied to each of these spectra and the resulting statistical uncertainty in each bin was obtained from a covariance matrix corresponding to the ensemble. To cross-check the correlation of the statistical uncertainties of the bin contents of the jet spectrum, the statistical uncertainties were also evaluated using the Bootstrap method [65, 66] and found to be consistent with the pseudo-random experiments. When calculating the ratio of jet cross sections, the spectra which appear in the numerator and denominator are from the same input data. The degree of correlation between the same p_{T} bins is nevertheless suppressed since jets reconstructed with different R may fall in different p_{T} bins. Thus the correlation was not taken into account; the numerator and denominator are treated as independent, which leads to a conservative estimate of the statistical uncertainties.

3.3 Systematic uncertainties

The systematic uncertainties of the p_T -differential charged-particle jet cross section and $R_{pPb}^{\text{ch jet}}$ are quantified by varying several parameters with respect to the primary analysis. The uncertainties are categorized based on their point-to-point correlation into correlated uncertainty, shape uncertainty, and normalization uncertainty. The correlated uncertainty is positively correlated among all the $p_{T,\text{jet}}^{\text{ch}}$ bins. It includes the uncertainty on the tracking efficiency and the uncertainty on the jet momentum smearing due to local background fluctuations. The shape uncertainty is the uncertainty which is anti-correlated between parts of the unfolded spectrum, which affects the shape of the final $p_{T,\text{jet}}^{\text{ch}}$ spectrum. It arises mainly due to assumptions in the unfolding procedure. The normalization uncertainties on the luminosity measurement, as described in Sec. 2, were determined to be 2.34% [36] and 3.7% [37] for pp and p–Pb collisions, respectively.

The influence of the statistical fluctuations on the systematic uncertainties of the raw spectrum was suppressed by using pseudo-experiments as done in Refs. [40, 63]. For each source of uncertainty, several randomized instances of the raw jet $p_{T,\text{jet}}^{\text{ch}}$ spectrum were generated by variations around the measured central value in each bin using a Gaussian distribution, with σ taken to be the uncorrelated statistical error in the bin. Each randomized instance was analyzed using (i) corrections for the primary analysis, and (ii) corrections that include the systematic variation. For each randomized instance, the ratio of corrected jet $p_{T,\text{jet}}^{\text{ch}}$ spectra resulting from (ii) and (i) was formed. The systematic uncertainty in each $p_{T,\text{jet}}^{\text{ch}}$ bin was defined as the mean value of the distribution of ratios obtained from all randomized instances. The uncertainties were taken as symmetric and the total uncertainty for each category was obtained by making a quadratic sum of the uncertainties corresponding to individual sources. The summary of the relative systematic uncertainties discussed in this section is presented in Table 1.

3.3.1 Correlated uncertainties

The main sources of correlated uncertainties are described below.

- **Tracking efficiency:** The dominant systematic uncertainty arises from the uncertainty on the ALICE tracking efficiency, which composes of two parts. The first part was estimated by simultaneously varying track selection criteria in the TPC in data and the MC simulation. The second one was determined by the discrepancy in the TPC-ITS track matching efficiency between data and simulations. The uncertainty on the inclusive p_T spectrum of charged particles was found to be 3% in pp collisions [67]. In p–Pb collisions, the value was found to increase with p_T from 1% at low p_T (~ 0.5 GeV/ c) up to 2.5% at high p_T (~ 14 GeV/ c). To assess how this uncertainty impacts the charged-particle jet spectrum, the unfolding was also performed with a response matrix which accounted for the lower track reconstruction efficiency. The difference between the jet spectrum obtained with the modified response matrix and the default one is adopted as the uncertainty on tracking efficiency.
- **PYTHIA fragmentation:** The instrumental response matrix used in the unfolding correction was built using PYTHIA simulations. The impact of the hadronization model in PYTHIA was assessed using the jet angularity observable. The jet angularity is defined as $g = \sum_i (p_{T,i} \times r_i) / p_{T,\text{jet}}^{\text{ch}}$, where $p_{T,i}$ is the p_T of the i^{th} constituent of the charged-particle jet and $r_i = \sqrt{\Delta\eta_i^2 + \Delta\phi_i^2}$ is the distance of the i^{th} constituent from the jet axis at the particle level. The angularity distribution was simulated using PYTHIA8 and HERWIG7 [68, 69] simulations. The corresponding jet angularity distributions differ up to about 30%. To assess the uncertainty associated with the detector effects on the fragmentation model, the instrumental response matrix was re-weighted according to the jet angularity. Specifically, the instrumental response matrix was re-weighted such that the 50% largest angularity jets were weighted an additional $\pm 30\%$ relative to the 50% lowest angularity

jets [26]. The modified response matrix was then used to unfold the measured spectrum. The difference between the unfolded jet spectrum obtained with the re-weighted response matrix and the default one is taken as the uncertainty.

- Background fluctuations: In p–Pb collisions, the δp_T matrix was constructed with cones perpendicular to the leading jet, as described in Section 3.2. The uncertainty on background fluctuations is estimated by taking the difference between the resulting jet spectrum and the default one.

3.3.2 Shape uncertainties

The main sources of the shape uncertainties are described below.

- Variation of the unfolding algorithm: The $p_{T,\text{jet}}^{\text{ch}}$ spectrum was unfolded with the iterative Bayesian unfolding method.
- Variation of the regularization parameter: The regularization parameter k_{reg} in the SVD-based unfolding was varied by ± 1 with respect to the optimal value.
- Variation of the prior: The prior spectrum was changed to a p_T spectrum of jets calculated with POWHEG+PYTHIA8 simulations.
- Variation of the lower p_T spectrum cutoff: The minimum p_T of the measured jet spectrum used in the unfolding correction was required to be greater than σ^{RC} of the δp_T^{RC} distribution. The sensitivity of the unfolded result to combinatorial jets was tested by varying the lower range of the measured jet spectrum by ± 3 GeV/ c .

The systematic uncertainties on the cross section ratios between jet spectra obtained with different R values are determined using the same strategy as in previous ALICE measurements [26]. The numerator and denominator were varied simultaneously and compared to the default jet cross section ratio.

The shape uncertainties between the pp and p–Pb collision systems are considered uncorrelated and are fully propagated to the $R_{\text{pPb}}^{\text{ch jet}}$. Due to the partial correlation between the tracking efficiency uncertainties in pp and p–Pb collisions [19], the tracking efficiency uncertainty on the $R_{\text{pPb}}^{\text{ch jet}}$ is considered to be the maximum uncanceled part between the two collision systems.

4 Results

4.1 Inclusive charged-particle jet production cross section in pp and p–Pb collisions

The charged-particle jet cross sections are reported differentially in $p_{T,\text{jet}}^{\text{ch}}$ and η_{jet} as

$$\frac{d^2\sigma}{dp_{T,\text{jet}}^{\text{ch}}d\eta_{\text{jet}}} = \frac{1}{L} \frac{d^2N}{dp_{T,\text{jet}}^{\text{ch}}d\eta_{\text{jet}}}, \quad (5)$$

where $d^2N/dp_{T,\text{jet}}^{\text{ch}}d\eta_{\text{jet}}$ is the fully corrected p_T - and η -differential charged-particle jet yield. The integrated luminosity for minimum bias events is denoted by L , see Sec. 2.

The fully corrected charged-particle jet cross sections for $R = 0.2, 0.3,$ and 0.4 in pp and p–Pb collisions are shown in Figs. 1 and 2, respectively. The jet cross sections for larger jet resolution parameters are scaled by arbitrary factors described in the legend for better visibility. These results are compatible with the previous results from ALICE [19, 67] and cover a wider $p_{T,\text{jet}}^{\text{ch}}$ interval, and are consistent with the ALICE charged-particle jet measurements [25]. The measurements are compared to two theoretical predictions:

Table 1: Summary of the contributions to the relative systematic uncertainty for the charged-particle jet cross section in pp and p-Pb collisions, and $R_{\text{pPb}}^{\text{ch, jet}}$ for $R = 0.2, 0.3,$ and 0.4 . The uncertainties depend on the $p_{\text{T, jet}}^{\text{ch}}$ and the table shows representative values corresponding to the first and last $p_{\text{T, jet}}^{\text{ch}}$ interval for each jet resolution parameter. The contributions are assumed to be independent and are summed in quadrature, resulting in the total uncertainty. See text for details.

R	$p_{\text{T, jet}}^{\text{ch}}$ (GeV/c)	Correlated uncertainty (%)				Shape uncertainty (%)				Norm. (%)	
		Trk. eff.	Frag.	Bkg. fluc.	Total	Algo.	Reg. par.	Prior	Bin trunc.		Total
PP	0.2	10–20	5.3	2.1	—	5.7	0.06	0.07	0.15	0.47	0.50
		120–140	9.7	1.1	—	9.8	8.0	4.3	0.70	4.3	10
	0.3	10–20	6.3	1.5	—	6.5	0.04	0.05	0.43	0.51	0.67
		120–140	9.6	0.40	—	9.6	9.7	4.1	1.1	2.7	11
	0.4	10–20	7.3	2.4	—	7.7	0.08	0.12	0.06	0.44	0.47
		120–140	10	0.40	—	10	9.3	7	0.64	1.2	12
p-Pb	0.2	10–20	16	0.70	0.21	16	2.0	0.34	0.22	0.21	2.05
		140–160	4.6	0.80	1.3	4.8	11	3.9	1.4	3.9	12
	0.3	10–20	16	1.4	0.54	16	0.51	0.78	0.24	0.54	1.1
		140–160	7.7	1.5	0.36	7.9	8.8	4.2	1.7	1.9	10
	0.4	10–20	16	1.7	1.2	16	3.9	0.74	0.19	0.20	4.0
		140–160	9.3	0.60	0.16	9.3	3.3	3.3	3.2	3.3	6.6
$R_{\text{pPb}}^{\text{ch, jet}}$	0.2	10–20	5.3	2.2	0.21	5.8	2.0	0.35	0.55	0.51	2.2
		120–140	4.8	1.4	1.3	5.2	11	4.9	3.1	4.9	13
	0.3	10–20	6.3	2.1	0.54	6.7	0.51	0.78	0.49	0.75	1.3
		120–140	7.3	1.6	0.36	7.5	12	5.7	1.1	2.8	14
	0.4	10–20	7.3	3.0	1.2	8.0	3.9	0.75	0.20	0.49	4.0
		120–140	9.1	0.72	0.16	9.1	10	7.2	1.6	2.2	13

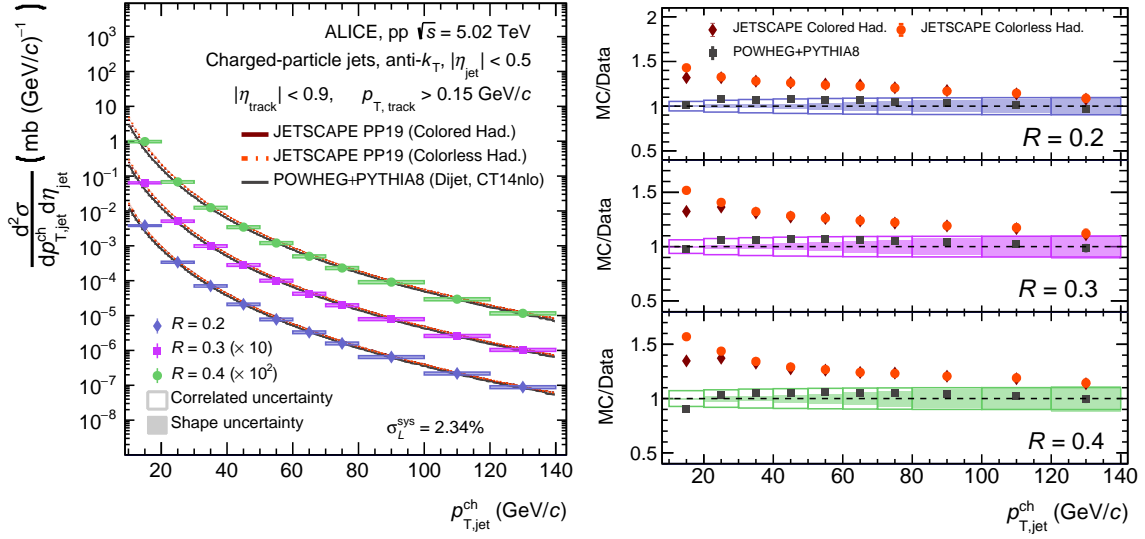


Figure 1: Left panel: Fully corrected charged-particle jet cross section in pp collisions at $\sqrt{s} = 5.02$ TeV for $R = 0.2, 0.3,$ and 0.4 (scale factors as indicated are used for better visibility). Statistical uncertainties are shown as vertical bars and are typically smaller than the marker size for all points. Boxes indicate systematic uncertainties. The additional normalization uncertainty due to luminosity is quoted separately as $\sigma_L^{\text{sys}} = 2.34\%$. The data are compared to the predictions by POWHEG+PYTHIA8 and JETSCAPE. Right panels: Ratio of the theory predictions to the measured data. The correlated and shape systematic uncertainties on the ratio account for the data uncertainties and do not show the normalization uncertainty.

- **POWHEG+PYTHIA8:** The matrix elements are computed at NLO accuracy with the POWHEG method [70, 71] using the dijet process [72] implemented in the POWHEG BOX V2 framework [73]. The POWHEG BOX is interfaced with the LHAPDF6 package [74] to supply different (n)PDF sets for describing the non-perturbative initial states, and PYTHIA8 [45] tune A14 [75] for parton shower and fragmentation. The simulation employs the CT14 NLO [76], TUJU21 NNLO [77], CTEQ6.1 NLO [78], and nNNPDF3.0 NLO [79] free-proton PDF sets. In the case of p–Pb collisions, the corresponding nPDF sets EPPS16 NLO [80], nTUJU21 NNLO [77], nCTEQ15WZSIH NLO [81, 82], and nNNPDF3.0 NLO [79] are used, accounting also for the shift in rapidity. The default values of α_s , renormalization, and factorization scales are adopted in the results shown in this paper.
- **JETSCAPE:** PYTHIA8 [45] is used to generate the initial hard scattering and the underlying event. The intermediate shower is handled by the MATTER [83, 84] model that includes parton virtuality. After parton shower, QCD strings are formed through either a colored or a colorless hadronization scheme. The strings are subsequently fed into PYTHIA8 for string fragmentation [85, 86]. The JETSCAPE configuration used in this paper is referred to as the PP19 tune [87] as implemented in JETSCAPE V3.4.1 [88]. The predictions are only shown for pp collisions.

As shown in the right panels of Figs. 1 and 2, within the uncertainties of the data, the POWHEG+PYTHIA8 predictions describe the data well, except for the lowest $p_{T,\text{jet}}^{\text{ch}}$ interval 10–20 GeV/c where a maximum discrepancy of $\sim 20\%$ is observed in both pp and p–Pb collisions. The JETSCAPE prediction in pp collisions overestimates the data by $\sim 50\%$ at low p_T . The magnitude of the discrepancy depends on the jet p_T and the resolution parameter R . The low- p_T region is sensitive to non-perturbative effects such as the initial state radiation and multiparton interactions. It is not clear to which extent can these discrepancies be explained by improper modelling of these effects.

The jet cross section ratios were evaluated by dividing the spectrum with $R = 0.2$ by those with other

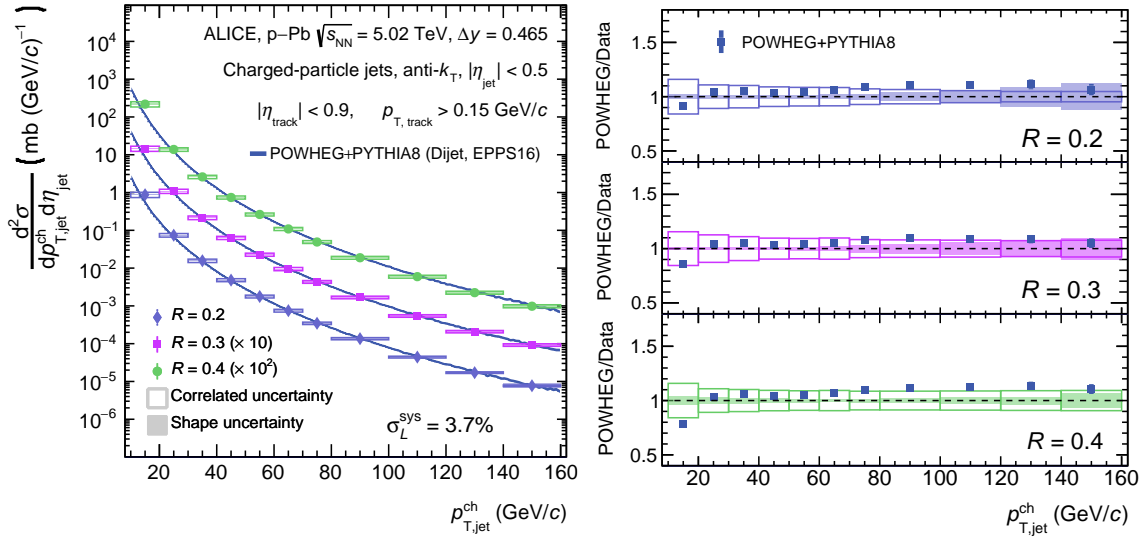


Figure 2: Similar results as Fig. 1 for p–Pb collisions at $\sqrt{s_{\text{NN}}} = 5.02$ TeV.

resolution parameters as shown in Fig. 3. The left panel is for pp collisions, and the right panel is for p–Pb collisions. In both pp and p–Pb collisions, the data are compared with the POWHEG+PYTHIA8 predictions. General agreement between data and POWHEG+PYTHIA8 predictions is observed within uncertainties. In pp collisions, the comparison between data and JETSCAPE predictions is also presented. JETSCAPE predictions are consistent with data within uncertainties as well, but they show a difference from the POWHEG+PYTHIA8 predictions at low $p_{\text{T, jet}}^{\text{ch}}$ in 20–40 GeV/c. The cross section ratio is sensitive to the collimation of particles around the jet axis and serves as an indirect measure of the jet structure [89]. Since the jet spectra in the numerator are always with a smaller jet resolution parameter R , it is expected that QCD radiation reduces this ratio below one, and that the effect decreases with the increasing collimation of jets at high p_{T} [33]. The ratios confirm the expected trend of increasing collimation with increasing transverse momentum of jets, corroborated also by the theoretical predictions. Figure 4 shows the comparison of the cross section ratios in pp collisions and p–Pb collisions. The comparison shows that the energy in the jet cone distributed transverse to the jet axis in p–Pb collisions is consistent with that in pp collisions. No sign of a modified jet structure is observed within uncertainties.

4.2 Nuclear modification factor $R_{\text{pPb}}^{\text{ch jet}}$

The nuclear modification factor of charged-particle jets in minimum bias p–Pb collisions due to nuclear matter effects is quantified by comparing the jet cross section in p–Pb collisions normalized by the number of nucleons of the Pb ion, $A = 208$, to the jet cross section in pp collisions, known as the A -scaling hypothesis [12, 90],

$$R_{\text{pPb}}^{\text{ch jet}} = \frac{1}{A} \frac{d^2 \sigma_{\text{pPb}}}{dp_{\text{T, jet}}^{\text{ch}} d\eta_{\text{jet}}} \bigg/ \frac{d^2 \sigma_{\text{pp}}}{dp_{\text{T, jet}}^{\text{ch}} d\eta_{\text{jet}}}. \quad (6)$$

The jet cross sections are measured in the laboratory frame with $|\eta_{\text{jet}}| < 0.5$ in both pp and p–Pb collisions. As mentioned above, the laboratory frame is shifted from the center-of-mass frame in rapidity by $\Delta y = 0.465$ in p–Pb collisions while it is not shifted for pp collisions, resulting in different jet rapidity acceptances in the center-of-mass frame between the two systems. However, this effect on $R_{\text{pPb}}^{\text{ch jet}}$ is smaller than 5% [19], and it is not accounted in Eq. (6).

Figure 5 depicts the nuclear modification factors $R_{\text{pPb}}^{\text{ch jet}}$ for jets with $R = 0.2, 0.3,$ and 0.4 as a function of jet transverse momentum. The $R_{\text{pPb}}^{\text{ch jet}}$ is compatible with one within uncertainties in the reported transverse momentum range $10 < p_{\text{T, jet}}^{\text{ch}} < 140$ GeV/c, and it is noted to be approximately independent of

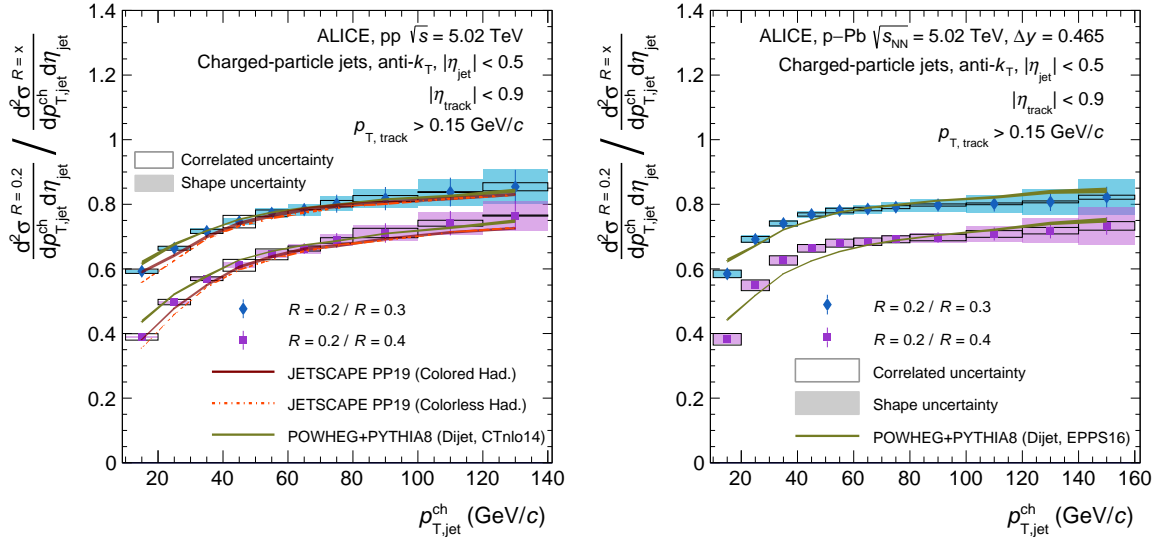


Figure 3: Fully corrected charged-particle jet cross section ratios with $R = 0.2$ to other jet resolution parameters. The plots also include comparison to the POWHEG+PYTHIA8 and JETSCAPE (in case of pp collisions) predictions. Left panel: pp collisions at $\sqrt{s} = 5.02$ TeV. Right panel: p–Pb collisions at $\sqrt{s_{NN}} = 5.02$ TeV.

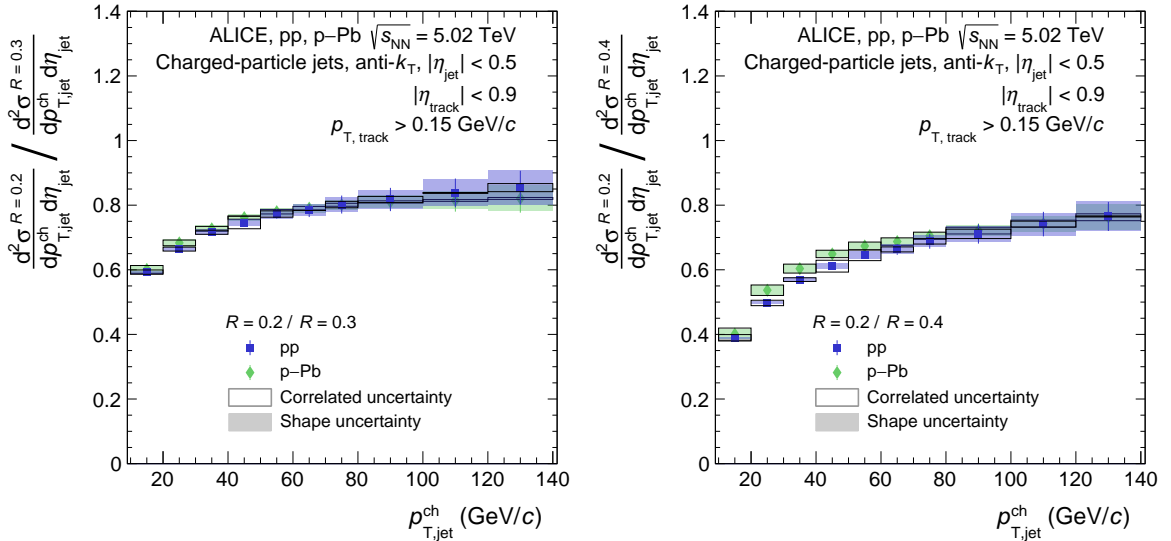


Figure 4: Comparison of jet cross section ratios between pp collisions and p–Pb collisions at $\sqrt{s_{NN}} = 5.02$ TeV. The left panel shows the ratios between jets with $R = 0.2$ and $R = 0.3$, the right panel shows the ratios between jets with $R = 0.2$ and $R = 0.4$.

jet transverse momentum and jet resolution parameter. The $R_{pPb}^{ch, jet}$ presented in this article is in agreement with the Run 1 result [19] within uncertainties. The results also indicate that jet quenching, if present, is below the sensitivity of the current measurement. The POWHEG+PYTHIA8 prediction calculated using the nCTEQ15WZSIH is found to best describe the data within uncertainties. This shows that the effects of nuclear-modified PDFs introduced by the nPDFs have minor impact on jet production. The data from this measurement can provide an important constraint on the global analysis of nPDFs.

The $R_{pPb}^{ch, jet}$ result reported in this paper is compared to other published experimental results currently available. Figure 6 shows the comparison to the measurement of full jets in p–Pb collisions at $\sqrt{s_{NN}} = 5.02$ TeV by the ATLAS [20] and CMS Collaborations [21] at the LHC, and d–Au collisions at $\sqrt{s_{NN}} =$

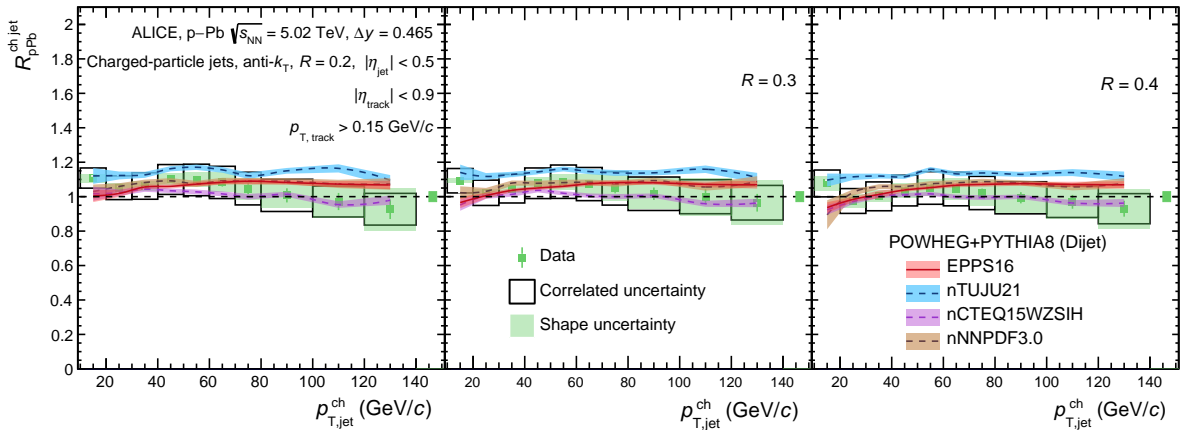


Figure 5: The nuclear modification factor $R_{pPb}^{ch,jet}$ of inclusive charged-particle jets as a function of $p_{T,jet}^{ch}$ at $\sqrt{s_{NN}} = 5.02$ TeV for $R = 0.2, 0.3,$ and 0.4 . The data measured are compared with the POWHEG+PYTHIA8 predictions calculated with various nPDFs. The bands on the predictions represent statistical uncertainties. Systematic and statistical uncertainties of data are shown as boxes and error bars, respectively. The normalization uncertainty of 4.37% is shown as a box around one.

200 GeV by the PHENIX Collaboration [22] at RHIC. Full jets are reconstructed with charged and neutral components. It is important to realize that the energy scales of the ATLAS, CMS, PHENIX, and ALICE measurements are different (jets measured by ALICE do not include neutral fragments) which complicates a direct comparison between the measurements. The ATLAS and CMS measurements show a hint of enhancement above one, but it has to be confirmed with higher precision measurements. It is worth noticing that by assuming the final state particles are dominated by pions, one can roughly estimate a scaling factor of around 1.5 between the energy of charged-particle jets and that of full jets. In general, the ALICE measurement is in qualitative agreement with those from ATLAS and CMS within the current experimental precision. The ALICE results shown here extend the measurements down to a jet p_T of 10 GeV/c and complement the measurements of the ATLAS and CMS Collaborations.

5 Conclusion

The inclusive p_T -differential charged-particle jet production cross sections in pp and p–Pb collisions at $\sqrt{s_{NN}} = 5.02$ TeV were measured using the ALICE detector at the LHC. The inclusive charged-particle jets were reconstructed with resolution parameters $R = 0.2, 0.3,$ and 0.4 . The measured charged-particle jet cross sections are corrected for experimental effects, such as the finite detector resolution on the jet energy scale as well as the effects of the uncorrelated background and its fluctuations. The ratios of jet cross sections measured for different values of R in pp collisions are consistent with those in p–Pb collisions within uncertainties, indicating no sign of jet structure modification in p–Pb collisions within the current measurement precision. Besides, the results confirm that the higher- p_T jets are more collimated. The cross section ratios also provide additional comparisons to theoretical predictions.

Within the current experimental precision and uncertainties, the nuclear modification factor $R_{pPb}^{ch,jet}$ is observed to be consistent with one, implying that the nuclear effects on jet production in p–Pb collisions are below the resolution of the current measurement. The $R_{pPb}^{ch,jet}$ is also found to be approximately independent of the jet resolution parameter, and is consistent with the measurements of full jets by the ATLAS, CMS, and PHENIX Collaborations within the kinematic region of overlap among the different measurements. The ALICE results reported in this paper extend the jet p_T reach down to 10 GeV/c and are thus complementary to those obtained with ATLAS and CMS.

The results are well described by NLO POWHEG+PYTHIA8 predictions (for pp and p–Pb collisions),

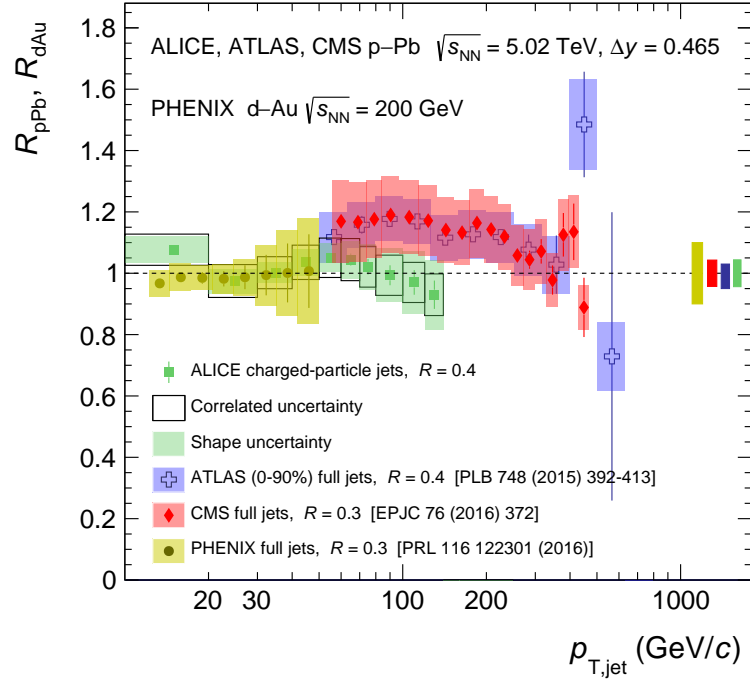


Figure 6: Comparison of the nuclear modification factors of jets in p–Pb and d–Au measurements at the LHC and RHIC, respectively. The boxes around the data points denote the systematic uncertainties, while the error bars denote the statistical uncertainties. The systematic uncertainties on the normalization are shown as boxes at $R_{pPb} = 1$.

while the JETSCAPE (for pp collisions) prediction agrees better with the data at high p_T . These results provide a constraint on initial- and final-state effects in nuclear collisions, global analysis of nPDF, and provide a new baseline for the study of jet production in heavy-ion collisions.

Acknowledgements

The ALICE Collaboration would like to thank all its engineers and technicians for their invaluable contributions to the construction of the experiment and the CERN accelerator teams for the outstanding performance of the LHC complex. The ALICE Collaboration gratefully acknowledges the resources and support provided by all Grid centres and the Worldwide LHC Computing Grid (WLCG) collaboration. The ALICE Collaboration acknowledges the following funding agencies for their support in building and running the ALICE detector: A. I. Alikhanyan National Science Laboratory (Yerevan Physics Institute) Foundation (ANSL), State Committee of Science and World Federation of Scientists (WFS), Armenia; Austrian Academy of Sciences, Austrian Science Fund (FWF): [M 2467-N36] and Nationalstiftung für Forschung, Technologie und Entwicklung, Austria; Ministry of Communications and High Technologies, National Nuclear Research Center, Azerbaijan; Conselho Nacional de Desenvolvimento Científico e Tecnológico (CNPq), Financiadora de Estudos e Projetos (Finep), Fundação de Amparo à Pesquisa do Estado de São Paulo (FAPESP) and Universidade Federal do Rio Grande do Sul (UFRGS), Brazil; Bulgarian Ministry of Education and Science, within the National Roadmap for Research Infrastructures 2020-2027 (object CERN), Bulgaria; Ministry of Education of China (MOEC), Ministry of Science & Technology of China (MSTC) and National Natural Science Foundation of China (NSFC), China; Ministry of Science and Education and Croatian Science Foundation, Croatia; Centro de Aplicaciones Tecnológicas y Desarrollo Nuclear (CEADEN), Cubaenergía, Cuba; Ministry of Education, Youth and Sports of the Czech Republic, Czech Republic; The Danish Council for Independent Research | Natural Sciences, the VILLUM FONDEN and Danish National Research Foundation (DNRF),

Denmark; Helsinki Institute of Physics (HIP), Finland; Commissariat à l’Energie Atomique (CEA) and Institut National de Physique Nucléaire et de Physique des Particules (IN2P3) and Centre National de la Recherche Scientifique (CNRS), France; Bundesministerium für Bildung und Forschung (BMBF) and GSI Helmholtzzentrum für Schwerionenforschung GmbH, Germany; General Secretariat for Research and Technology, Ministry of Education, Research and Religions, Greece; National Research, Development and Innovation Office, Hungary; Department of Atomic Energy Government of India (DAE), Department of Science and Technology, Government of India (DST), University Grants Commission, Government of India (UGC) and Council of Scientific and Industrial Research (CSIR), India; National Research and Innovation Agency - BRIN, Indonesia; Istituto Nazionale di Fisica Nucleare (INFN), Italy; Japanese Ministry of Education, Culture, Sports, Science and Technology (MEXT) and Japan Society for the Promotion of Science (JSPS) KAKENHI, Japan; Consejo Nacional de Ciencia (CONACYT) y Tecnología, through Fondo de Cooperación Internacional en Ciencia y Tecnología (FONCICYT) and Dirección General de Asuntos del Personal Académico (DGAPA), Mexico; Nederlandse Organisatie voor Wetenschappelijk Onderzoek (NWO), Netherlands; The Research Council of Norway, Norway; Commission on Science and Technology for Sustainable Development in the South (COMSATS), Pakistan; Pontificia Universidad Católica del Perú, Peru; Ministry of Education and Science, National Science Centre and WUT ID-UB, Poland; Korea Institute of Science and Technology Information and National Research Foundation of Korea (NRF), Republic of Korea; Ministry of Education and Scientific Research, Institute of Atomic Physics, Ministry of Research and Innovation and Institute of Atomic Physics and University Politehnica of Bucharest, Romania; Ministry of Education, Science, Research and Sport of the Slovak Republic, Slovakia; National Research Foundation of South Africa, South Africa; Swedish Research Council (VR) and Knut & Alice Wallenberg Foundation (KAW), Sweden; European Organization for Nuclear Research, Switzerland; Suranaree University of Technology (SUT), National Science and Technology Development Agency (NSTDA), Thailand Science Research and Innovation (TSRI) and National Science, Research and Innovation Fund (NSRF), Thailand; Turkish Energy, Nuclear and Mineral Research Agency (TENMAK), Turkey; National Academy of Sciences of Ukraine, Ukraine; Science and Technology Facilities Council (STFC), United Kingdom; National Science Foundation of the United States of America (NSF) and United States Department of Energy, Office of Nuclear Physics (DOE NP), United States of America. In addition, individual groups or members have received support from: European Research Council, Strong 2020 - Horizon 2020 (grant nos. 950692, 824093), European Union; Academy of Finland (Center of Excellence in Quark Matter) (grant nos. 346327, 346328), Finland.

References

- [1] M. Dasgupta, F. A. Dreyer, G. P. Salam, and G. Soyez, “Inclusive jet spectrum for small-radius jets”, *JHEP* **06** (2016) 057, arXiv:1602.01110 [hep-ph].
- [2] Z.-B. Kang, F. Ringer, and I. Vitev, “The semi-inclusive jet function in SCET and small radius resummation for inclusive jet production”, *JHEP* **10** (2016) 125, arXiv:1606.06732 [hep-ph].
- [3] X. Liu, S.-O. Moch, and F. Ringer, “Threshold and jet radius joint resummation for single-inclusive jet production”, *Phys. Rev. Lett.* **119** (2017) 212001, arXiv:1708.04641 [hep-ph].
- [4] J. Currie, E. W. N. Glover, and J. Pires, “Next-to-Next-to Leading Order QCD Predictions for Single Jet Inclusive Production at the LHC”, *Phys. Rev. Lett.* **118** (2017) 072002, arXiv:1611.01460 [hep-ph].
- [5] I. Vitev, “Initial state parton broadening and energy loss probed in d+Au at RHIC”, *Phys. Lett. B* **562** (2003) 36–44, arXiv:nucl-th/0302002.

- [6] M. Connors, C. Nattrass, R. Reed, and S. Salur, “Jet measurements in heavy ion physics”, *Rev. Mod. Phys.* **90** (2018) 025005, arXiv:1705.01974 [nucl-ex].
- [7] W. Busza, K. Rajagopal, and W. van der Schee, “Heavy Ion Collisions: The Big Picture, and the Big Questions”, *Ann. Rev. Nucl. Part. Sci.* **68** (2018) 339–376, arXiv:1802.04801 [hep-ph].
- [8] B. V. Jacak and B. Muller, “The exploration of hot nuclear matter”, *Science* **337** (2012) 310–314.
- [9] ALICE Collaboration, “The ALICE experiment – A journey through QCD”, arXiv:2211.04384 [nucl-ex].
- [10] M. Gyulassy and M. Plümer, “Jet quenching in dense matter”, *Phys. Lett. B* **243** (1990) 432–438.
- [11] G.-Y. Qin and X.-N. Wang, “Jet quenching in high-energy heavy-ion collisions”, *Int. J. Mod. Phys.* **24** (2015) E1530014, arXiv:1511.00790 [hep-ph].
- [12] M. L. Miller, K. Reygers, S. J. Sanders, and P. Steinberg, “Glauber modeling in high energy nuclear collisions”, *Ann. Rev. Nucl. Part. Sci.* **57** (2007) 205–243, arXiv:nucl-ex/0701025.
- [13] ALICE Collaboration, B. B. Abelev *et al.*, “Multiparticle azimuthal correlations in p–Pb and Pb–Pb collisions at the CERN Large Hadron Collider”, *Phys. Rev. C* **90** (2014) 054901, arXiv:1406.2474 [nucl-ex].
- [14] ALICE Collaboration, B. Abelev *et al.*, “Long-range angular correlations on the near and away side in p–Pb collisions at $\sqrt{s_{NN}} = 5.02$ TeV”, *Phys. Lett. B* **719** (2013) 29–41, arXiv:1212.2001 [nucl-ex].
- [15] ATLAS Collaboration, G. Aad *et al.*, “Observation of Associated Near-Side and Away-Side Long-Range Correlations in $\sqrt{s_{NN}} = 5.02$ TeV Proton-Lead Collisions with the ATLAS Detector”, *Phys. Rev. Lett.* **110** (2013) 182302, arXiv:1212.5198 [hep-ex].
- [16] CMS Collaboration, V. Khachatryan *et al.*, “Evidence for Collective Multiparticle Correlations in p–Pb Collisions”, *Phys. Rev. Lett.* **115** (2015) 012301, arXiv:1502.05382 [nucl-ex].
- [17] PHENIX Collaboration, A. Adare *et al.*, “Measurement of long-range angular correlation and quadrupole anisotropy of pions and (anti)protons in central d+Au collisions at $\sqrt{s_{NN}} = 200$ GeV”, *Phys. Rev. Lett.* **114** (2015) 192301, arXiv:1404.7461 [nucl-ex].
- [18] STAR Collaboration, L. Adamczyk *et al.*, “Effect of event selection on jetlike correlation measurement in d+Au collisions at $\sqrt{s_{NN}} = 200$ GeV”, *Phys. Lett. B* **743** (2015) 333–339, arXiv:1412.8437 [nucl-ex].
- [19] ALICE Collaboration, J. Adam *et al.*, “Measurement of charged jet production cross sections and nuclear modification in p–Pb collisions at $\sqrt{s_{NN}} = 5.02$ TeV”, *Phys. Lett. B* **749** (2015) 68–81, arXiv:1503.00681 [nucl-ex].
- [20] ATLAS Collaboration, G. Aad *et al.*, “Centrality and rapidity dependence of inclusive jet production in $\sqrt{s_{NN}} = 5.02$ TeV proton-lead collisions with the ATLAS detector”, *Phys. Lett. B* **748** (2015) 392–413, arXiv:1412.4092 [hep-ex].
- [21] CMS Collaboration, V. Khachatryan *et al.*, “Measurement of inclusive jet production and nuclear modifications in p–Pb collisions at $\sqrt{s_{NN}} = 5.02$ TeV”, *Eur. Phys. J. C* **76** (2016) 372, arXiv:1601.02001 [nucl-ex].
- [22] PHENIX Collaboration, A. Adare *et al.*, “Centrality-dependent modification of jet-production rates in deuteron-gold collisions at $\sqrt{s_{NN}} = 200$ GeV”, *Phys. Rev. Lett.* **116** (2016) 122301, arXiv:1509.04657 [nucl-ex].

- [23] **ALICE** Collaboration, K. Aamodt *et al.*, “Alignment of the ALICE Inner Tracking System with cosmic-ray tracks”, *JINST* **5** (2010) P03003, arXiv:1001.0502 [physics.ins-det].
- [24] **ALICE** Collaboration, B. Abelev *et al.*, “Performance of the ALICE Experiment at the CERN LHC”, *Int. J. Mod. Phys. A* **29** (2014) 1430044, arXiv:1402.4476 [nucl-ex].
- [25] **ALICE** Collaboration, S. Acharya *et al.*, “Measurement of the radius dependence of charged-particle jet suppression in Pb–Pb collisions at $\sqrt{s_{\text{NN}}} = 5.02$ TeV”, *Phys. Lett. B* **849** (2024) 138412, arXiv:2303.00592 [nucl-ex].
- [26] **ALICE** Collaboration, S. Acharya *et al.*, “Measurements of inclusive jet spectra in pp and central Pb–Pb collisions at $\sqrt{s_{\text{NN}}} = 5.02$ TeV”, *Phys. Rev. C* **101** (2020) 034911, arXiv:1909.09718 [nucl-ex].
- [27] **NNPDF** Collaboration, R. D. Ball *et al.*, “Precision determination of the strong coupling constant within a global PDF analysis”, *Eur. Phys. J. C* **78** (2018) 408, arXiv:1802.03398 [hep-ph].
- [28] **CMS** Collaboration, A. M. Sirunyan *et al.*, “Constraining gluon distributions in nuclei using dijets in proton-proton and proton-lead collisions at $\sqrt{s_{\text{NN}}} = 5.02$ TeV”, *Phys. Rev. Lett.* **121** (2018) 062002, arXiv:1805.04736 [hep-ex].
- [29] N. Armesto, H. Paukkunen, J. M. Penín, C. A. Salgado, and P. Zurita, “An analysis of the impact of LHC Run I proton–lead data on nuclear parton densities”, *Eur. Phys. J. C* **76** (2016) 218, arXiv:1512.01528 [hep-ph].
- [30] H. Paukkunen, “Nuclear PDFs in the beginning of the LHC era”, *Nucl. Phys. A* **926** (2014) 24–33, arXiv:1401.2345 [hep-ph].
- [31] D. Britzger, K. Rabbertz, D. Savoiu, G. Sieber, and M. Wobisch, “Determination of the strong coupling constant using inclusive jet cross section data from multiple experiments”, *Eur. Phys. J. C* **79** (2019) 68, arXiv:1712.00480 [hep-ph].
- [32] M. Dasgupta, L. Magnea, and G. P. Salam, “Non-perturbative QCD effects in jets at hadron colliders”, *JHEP* **02** (2008) 055, arXiv:0712.3014 [hep-ph].
- [33] **CMS** Collaboration, S. Chatrchyan *et al.*, “Measurement of the Ratio of Inclusive Jet Cross Sections using the Anti- k_T Algorithm with Radius Parameters $R = 0.5$ and 0.7 in pp Collisions at $\sqrt{s} = 7$ TeV”, *Phys. Rev. D* **90** (2014) 072006, arXiv:1406.0324 [hep-ex].
- [34] **CMS** Collaboration, A. M. Sirunyan *et al.*, “Dependence of inclusive jet production on the anti- k_T distance parameter in pp collisions at $\sqrt{s} = 13$ TeV”, *JHEP* **12** (2020) 082, arXiv:2005.05159 [hep-ex].
- [35] **ALICE** Collaboration, K. Aamodt *et al.*, “The ALICE experiment at the CERN LHC”, *JINST* **3** (2008) S08002.
- [36] **ALICE** Collaboration, S. Acharya *et al.*, “ALICE 2017 luminosity determination for pp collisions at $\sqrt{s} = 5$ TeV”, Tech. Rep. ALICE-PUBLIC-2018-014, 2018. <https://cds.cern.ch/record/2648933>.
- [37] **ALICE** Collaboration, B. Abelev *et al.*, “Measurement of visible cross sections in proton-lead collisions at $\sqrt{s_{\text{NN}}} = 5.02$ TeV in van der Meer scans with the ALICE detector”, *JINST* **9** (2014) P11003, arXiv:1405.1849 [nucl-ex].
- [38] **ALICE** Collaboration, J. Adam *et al.*, “Centrality dependence of particle production in p–Pb collisions at $\sqrt{s_{\text{NN}}} = 5.02$ TeV”, *Phys. Rev. C* **91** (2015) 064905, arXiv:1412.6828 [nucl-ex].

- [39] **ALICE** Collaboration, E. Abbas *et al.*, “Performance of the ALICE VZERO system”, *JINST* **8** (2013) P10016, arXiv:1306.3130 [nucl-ex].
- [40] **ALICE** Collaboration, S. Acharya *et al.*, “Measurement of inclusive charged-particle b-jet production in pp and p–Pb collisions at $\sqrt{s_{NN}} = 5.02$ TeV”, *JHEP* **01** (2022) 178, arXiv:2110.06104 [nucl-ex].
- [41] **ALICE** Collaboration, S. Acharya *et al.*, “The ALICE definition of primary particles”, Tech. Rep. ALICE-PUBLIC-2017-005, 2017. <https://cds.cern.ch/record/2270008>.
- [42] J. Alme *et al.*, “The ALICE TPC, a large 3-dimensional tracking device with fast readout for ultra-high multiplicity events”, *Nucl. Instrum. Meth. A* **622** (2010) 316–367, arXiv:1001.1950 [physics.ins-det].
- [43] **ALICE** Collaboration, B. Abelev *et al.*, “Measurement of charged jet suppression in Pb–Pb collisions at $\sqrt{s_{NN}} = 2.76$ TeV”, *JHEP* **03** (2014) 013, arXiv:1311.0633 [nucl-ex].
- [44] R. Brun, F. Bruyant, F. Carminati, S. Giani, M. Maire, A. McPherson, G. Patrick, and L. Urban, *GEANT: Detector Description and Simulation Tool; Oct 1994*. CERN Program Library. CERN, Geneva, 1993. <https://cds.cern.ch/record/1082634>. Long Writeup W5013.
- [45] T. Sjöstrand *et al.*, “An introduction to PYTHIA 8.2”, *Comput. Phys. Commun.* **191** (2015) 159–177, arXiv:1410.3012 [hep-ph].
- [46] P. Skands, S. Carrazza, and J. Rojo, “Tuning PYTHIA 8.1: the Monash 2013 Tune”, *Eur. Phys. J. C* **74** (2014) 3024, arXiv:1404.5630 [hep-ph].
- [47] T. Sjostrand, S. Mrenna, and P. Z. Skands, “PYTHIA 6.4 Physics and Manual”, *JHEP* **05** (2006) 026, arXiv:hep-ph/0603175.
- [48] P. Z. Skands, “Tuning Monte Carlo Generators: The Perugia Tunes”, *Phys. Rev. D* **82** (2010) 074018, arXiv:1005.3457 [hep-ph].
- [49] M. Cacciari, G. P. Salam, and G. Soyez, “FastJet User Manual”, *Eur. Phys. J. C* **72** (2012) 1896, arXiv:1111.6097 [hep-ph].
- [50] M. Cacciari, G. P. Salam, and G. Soyez, “The anti- k_T jet clustering algorithm”, *JHEP* **04** (2008) 063, arXiv:0802.1189 [hep-ph].
- [51] M. Cacciari and G. P. Salam, “Pileup subtraction using jet areas”, *Phys. Lett. B* **659** (2008) 119–126, arXiv:0707.1378 [hep-ph].
- [52] **CMS** Collaboration, S. Chatrchyan *et al.*, “Measurement of the Underlying Event Activity in pp Collisions at $\sqrt{s} = 0.9$ and 7 TeV with the Novel Jet-Area/Median Approach”, *JHEP* **08** (2012) 130, arXiv:1207.2392 [hep-ex].
- [53] M. Cacciari, G. P. Salam, and G. Soyez, “The Catchment Area of Jets”, *JHEP* **04** (2008) 005, arXiv:0802.1188 [hep-ph].
- [54] M. Cacciari, J. Rojo, G. P. Salam, and G. Soyez, “Jet Reconstruction in Heavy Ion Collisions”, *Eur. Phys. J. C* **71** (2011) 1539, arXiv:1010.1759 [hep-ph].
- [55] **ALICE** Collaboration, S. Acharya *et al.*, “Measurements of the groomed jet radius and momentum splitting fraction with the soft drop and dynamical grooming algorithms in pp collisions at $\sqrt{s} = 5.02$ TeV”, *JHEP* **05** (2023) 244, arXiv:2204.10246 [nucl-ex].

- [56] V. Blobel, “Unfolding methods in particle physics”, in *Proceedings, PHYSTAT 2011 Workshop, CERN, Geneva, Switzerland, January 2011, CERN-2011-006*, pp. 240–251. 2011.
- [57] G. Cowan, “A survey of unfolding methods for particle physics”, *Conf. Proc. C* **0203181** (2002) 248–257.
- [58] ALICE Collaboration, J. Adam *et al.*, “Measurement of jet suppression in central Pb–Pb collisions at $\sqrt{s_{NN}} = 2.76$ TeV”, *Phys. Lett. B* **746** (2015) 1–14, arXiv:1502.01689 [nucl-ex].
- [59] R. Brun, F. Bruyant, M. Maire, A. C. McPherson, and P. Zancarini, *GEANT 3: user’s guide Geant 3.10, Geant 3.11; rev. version*. CERN, Geneva, 1987. <https://cds.cern.ch/record/1119728>.
- [60] ALICE Collaboration, B. Abelev *et al.*, “Measurement of Event Background Fluctuations for Charged Particle Jet Reconstruction in Pb–Pb collisions at $\sqrt{s_{NN}} = 2.76$ TeV”, *JHEP* **03** (2012) 053, arXiv:1201.2423 [hep-ex].
- [61] A. Hocker and V. Kartvelishvili, “SVD approach to data unfolding”, *Nucl. Instrum. Meth. A* **372** (1996) 469–481, arXiv:hep-ph/9509307.
- [62] G. D’Agostini, “A Multidimensional unfolding method based on Bayes’ theorem”, *Nucl. Instrum. Meth. A* **362** (1995) 487–498.
- [63] ALICE Collaboration, S. Acharya *et al.*, “Constraints on jet quenching in p–Pb collisions at $\sqrt{s_{NN}} = 5.02$ TeV measured by the event-activity dependence of semi-inclusive hadron-jet distributions”, *Phys. Lett. B* **783** (2018) 95–113, arXiv:1712.05603 [nucl-ex].
- [64] T. Adye, “Unfolding algorithms and tests using RooUnfold”, in *Proceedings, PHYSTAT 2011 Workshop, CERN, Geneva, Switzerland, January 2011, CERN-2011-006*, pp. 313–318. 2011. arXiv:1105.1160 [physics.data-an].
- [65] B. Efron, “Bootstrap Methods: Another Look at the Jackknife”, *Annals Statist.* **7** (1979) 1–26.
- [66] ATLAS Collaboration, M. Aaboud *et al.*, “Measurement of inclusive jet and dijet cross-sections in proton-proton collisions at $\sqrt{s} = 13$ TeV with the ATLAS detector”, *JHEP* **05** (2018) 195, arXiv:1711.02692 [hep-ex].
- [67] ALICE Collaboration, S. Acharya *et al.*, “Measurement of charged jet cross section in pp collisions at $\sqrt{s} = 5.02$ TeV”, *Phys. Rev. D* **100** (2019) 092004, arXiv:1905.02536 [nucl-ex].
- [68] M. Bahr *et al.*, “Herwig++ Physics and Manual”, *Eur. Phys. J. C* **58** (2008) 639–707, arXiv:0803.0883 [hep-ph].
- [69] J. Bellm *et al.*, “Herwig 7.0/Herwig++ 3.0 release note”, *Eur. Phys. J. C* **76** (2016) 196, arXiv:1512.01178 [hep-ph].
- [70] S. Frixione, P. Nason, and C. Oleari, “Matching NLO QCD computations with Parton Shower simulations: the POWHEG method”, *JHEP* **11** (2007) 070, arXiv:0709.2092 [hep-ph].
- [71] P. Nason, “A New method for combining NLO QCD with shower Monte Carlo algorithms”, *JHEP* **11** (2004) 040, arXiv:hep-ph/0409146.
- [72] S. Alioli, K. Hamilton, P. Nason, C. Oleari, and E. Re, “Jet pair production in POWHEG”, *JHEP* **04** (2011) 081, arXiv:1012.3380 [hep-ph].
- [73] S. Alioli, P. Nason, C. Oleari, and E. Re, “A general framework for implementing NLO calculations in shower Monte Carlo programs: the POWHEG BOX”, *JHEP* **06** (2010) 043, arXiv:1002.2581 [hep-ph].

- [74] A. Buckley, J. Ferrando, S. Lloyd, K. Nordström, B. Page, M. Rüfenacht, M. Schönherr, and G. Watt, “LHAPDF6: parton density access in the LHC precision era”, *Eur. Phys. J. C* **75** (2015) 132, arXiv:1412.7420 [hep-ph].
- [75] ATLAS Collaboration, “ATLAS PYTHIA 8 tunes to 7 TeV data.” ATL-PHYS-PUB-2014-021, 2014. <https://cds.cern.ch/record/1966419>.
- [76] S. Dulat, T.-J. Hou, J. Gao, M. Guzzi, J. Huston, P. Nadolsky, J. Pumplin, C. Schmidt, D. Stump, and C. P. Yuan, “New parton distribution functions from a global analysis of quantum chromodynamics”, *Phys. Rev. D* **93** (2016) 033006, arXiv:1506.07443 [hep-ph].
- [77] I. Helenius, M. Walt, and W. Vogelsang, “NNLO nuclear parton distribution functions with electroweak-boson production data from the LHC”, *Phys. Rev. D* **105** (2022) 094031, arXiv:2112.11904 [hep-ph].
- [78] D. Stump, J. Huston, J. Pumplin, W.-K. Tung, H. L. Lai, S. Kuhlmann, and J. F. Owens, “Inclusive jet production, parton distributions, and the search for new physics”, *JHEP* **10** (2003) 046, arXiv:hep-ph/0303013.
- [79] R. Abdul Khalek, R. Gauld, T. Giani, E. R. Nocera, T. R. Rabemananjara, and J. Rojo, “nNNPDF3.0: evidence for a modified partonic structure in heavy nuclei”, *Eur. Phys. J. C* **82** (2022) 507, arXiv:2201.12363 [hep-ph].
- [80] K. J. Eskola, P. Paakkinen, H. Paukkunen, and C. A. Salgado, “EPPS16: Nuclear parton distributions with LHC data”, *Eur. Phys. J. C* **77** (2017) 163, arXiv:1612.05741 [hep-ph].
- [81] K. Kovarik *et al.*, “nCTEQ15 - Global analysis of nuclear parton distributions with uncertainties in the CTEQ framework”, *Phys. Rev. D* **93** (2016) 085037, arXiv:1509.00792 [hep-ph].
- [82] A. Kusina *et al.*, “Impact of LHC vector boson production in heavy ion collisions on strange PDFs”, *Eur. Phys. J. C* **80** (2020) 968, arXiv:2007.09100 [hep-ph].
- [83] A. Majumder, “Incorporating Space-Time Within Medium-Modified Jet Event Generators”, *Phys. Rev. C* **88** (2013) 014909, arXiv:1301.5323 [nucl-th].
- [84] S. Cao and A. Majumder, “Nuclear modification of leading hadrons and jets within a virtuality ordered parton shower”, *Phys. Rev. C* **101** (2020) 024903, arXiv:1712.10055 [nucl-th].
- [85] B. Andersson, G. Gustafson, G. Ingelman, and T. Sjostrand, “Parton Fragmentation and String Dynamics”, *Phys. Rept.* **97** (1983) 31–145.
- [86] B. Andersson, *The Lund model*, vol. 7. Cambridge University Press, 7, 2005.
- [87] JETSCAPE Collaboration, A. Kumar *et al.*, “JETSCAPE framework: $p + p$ results”, *Phys. Rev. C* **102** (2020) 054906, arXiv:1910.05481 [nucl-th].
- [88] J. H. Putschke *et al.*, “The JETSCAPE framework”, arXiv:1903.07706 [nucl-th].
- [89] G. Soyez, “A Simple description of jet cross-section ratios”, *Phys. Lett. B* **698** (2011) 59–62, arXiv:1101.2665 [hep-ph].
- [90] CMS Collaboration, A. Tumasyan *et al.*, “Nuclear modification of Υ states in pPb collisions at $\sqrt{s_{NN}} = 5.02$ TeV”, *Phys. Lett. B* **835** (2022) 137397, arXiv:2202.11807 [hep-ex].

A The ALICE Collaboration

S. Acharya ¹²⁸, D. Adamová ⁸⁷, A. Adler⁷¹, G. Aglieri Rinella ³³, M. Agnello ³⁰, N. Agrawal ⁵², Z. Ahammed ¹³⁶, S. Ahmad ¹⁶, S.U. Ahn ⁷², I. Ahuja ³⁸, A. Akindinov ¹⁴², M. Al-Turany ⁹⁸, D. Aleksandrov ¹⁴², B. Alessandro ⁵⁷, H.M. Alfanda ⁶, R. Alfaro Molina ⁶⁸, B. Ali ¹⁶, A. Alici ²⁶, N. Alizadehvandchali ¹¹⁷, A. Alkin ³³, J. Alme ²¹, G. Alocco ⁵³, T. Alt ⁶⁵, A.R. Altamura ⁵¹, I. Altsybeev ⁹⁶, J.R. Alvarado ⁴⁵, M.N. Anaam ⁶, C. Andrei ⁴⁶, N. Andreou ¹¹⁶, A. Andronic ¹²⁷, V. Anguelov ⁹⁵, F. Antinori ⁵⁵, P. Antonioli ⁵², N. Apadula ⁷⁵, L. Aphecetche ¹⁰⁴, H. Appelshäuser ⁶⁵, C. Arata ⁷⁴, S. Arcelli ²⁶, M. Aresti ²³, R. Arnaldi ⁵⁷, J.G.M.C.A. Arneiro ¹¹¹, I.C. Arsene ²⁰, M. Arslanok ¹³⁹, A. Augustinus ³³, R. Averbeck ⁹⁸, M.D. Azmi ¹⁶, H. Baba¹²⁵, A. Badalà ⁵⁴, J. Bae ¹⁰⁵, Y.W. Baek ⁴¹, X. Bai ¹²¹, R. Bailhache ⁶⁵, Y. Bailung ⁴⁹, A. Balbino ³⁰, A. Baldisseri ¹³¹, B. Balis ², D. Banerjee ⁴, Z. Banoo ⁹², R. Barbera ²⁷, F. Barile ³², L. Barioglio ⁹⁶, M. Barlou⁷⁹, G.G. Barnaföldi ⁴⁷, L.S. Barnby ⁸⁶, V. Barret ¹²⁸, L. Barreto ¹¹¹, C. Bartels ¹²⁰, K. Barth ³³, E. Bartsch ⁶⁵, N. Bastid ¹²⁸, S. Basu ⁷⁶, G. Batigne ¹⁰⁴, D. Battistini ⁹⁶, B. Batyunya ¹⁴³, D. Bauri⁴⁸, J.L. Bazo Alba ¹⁰², I.G. Bearden ⁸⁴, C. Beattie ¹³⁹, P. Becht ⁹⁸, D. Behera ⁴⁹, I. Belikov ¹³⁰, A.D.C. Bell Hechavarria ¹²⁷, F. Bellini ²⁶, R. Bellwied ¹¹⁷, S. Belokurova ¹⁴², G. Bencedi ⁴⁷, S. Beole ²⁵, A. Bercuci ⁴⁶, Y. Berdnikov ¹⁴², A. Berdnikova ⁹⁵, L. Bergmann ⁹⁵, M.G. Besoiu ⁶⁴, L. Betev ³³, P.P. Bhaduri ¹³⁶, A. Bhasin ⁹², M.A. Bhat ⁴, B. Bhattacharjee ⁴², L. Bianchi ²⁵, N. Bianchi ⁵⁰, J. Bielčák ³⁶, J. Bielčiková ⁸⁷, J. Biernat ¹⁰⁸, A.P. Bigot ¹³⁰, A. Bilandzic ⁹⁶, G. Biro ⁴⁷, S. Biswas ⁴, N. Bize ¹⁰⁴, J.T. Blair ¹⁰⁹, D. Blau ¹⁴², M.B. Blidaru ⁹⁸, N. Bluhme³⁹, C. Blume ⁶⁵, G. Boca ^{22,56}, F. Bock ⁸⁸, T. Bodova ²¹, A. Bogdanov¹⁴², S. Boi ²³, J. Bok ⁵⁹, L. Boldizsár ⁴⁷, M. Bombara ³⁸, P.M. Bond ³³, G. Bonomi ^{135,56}, H. Borel ¹³¹, A. Borissov ¹⁴², A.G. Borquez Carcamo ⁹⁵, H. Bossi ¹³⁹, E. Botta ²⁵, Y.E.M. Bouziani ⁶⁵, L. Bratrud ⁶⁵, P. Braun-Munzinger ⁹⁸, M. Bregant ¹¹¹, M. Broz ³⁶, G.E. Bruno ^{97,32}, M.D. Buckland ²⁴, D. Budnikov ¹⁴², H. Buesching ⁶⁵, S. Bufalino ³⁰, P. Buhler ¹⁰³, N. Burmasov ¹⁴², Z. Buthelezi ^{69,124}, A. Bylinkin ²¹, S.A. Bysiak¹⁰⁸, M. Cai ⁶, H. Caines ¹³⁹, A. Caliva ²⁹, E. Calvo Villar ¹⁰², J.M.M. Camacho ¹¹⁰, P. Camerini ²⁴, F.D.M. Canedo ¹¹¹, S.L. Cantway ¹³⁹, M. Carabas ¹¹⁴, A.A. Carballo ³³, F. Carnesecchi ³³, R. Caron ¹²⁹, L.A.D. Carvalho ¹¹¹, J. Castillo Castellanos ¹³¹, F. Catalano ^{33,25}, C. Ceballos Sanchez ¹⁴³, I. Chakaberia ⁷⁵, P. Chakraborty ⁴⁸, S. Chandra ¹³⁶, S. Chapeland ³³, M. Chartier ¹²⁰, S. Chattopadhyay ¹³⁶, S. Chattopadhyay ¹⁰⁰, T. Cheng ^{98,6}, C. Cheshkov ¹²⁹, B. Cheynis ¹²⁹, V. Chibante Barroso ³³, D.D. Chinellato ¹¹², E.S. Chizzali ^{11,96}, J. Cho ⁵⁹, S. Cho ⁵⁹, P. Chochula ³³, P. Christakoglou ⁸⁵, C.H. Christensen ⁸⁴, P. Christiansen ⁷⁶, T. Chujo ¹²⁶, M. Ciacco ³⁰, C. Cicalo ⁵³, F. Cindolo ⁵², M.R. Ciupek⁹⁸, G. Clai^{III,52}, F. Colamaria ⁵¹, J.S. Colburn¹⁰¹, D. Colella ^{97,32}, M. Colocci ²⁶, M. Concas ^{IV,57}, G. Conesa Balbastre ⁷⁴, Z. Conesa del Valle ¹³², G. Contin ²⁴, J.G. Contreras ³⁶, M.L. Coquet ¹³¹, P. Cortese ^{134,57}, M.R. Cosentino ¹¹³, F. Costa ³³, S. Costanza ^{22,56}, C. Cot ¹³², J. Crkovská ⁹⁵, P. Crochet ¹²⁸, R. Cruz-Torres ⁷⁵, P. Cui ⁶, A. Dainese ⁵⁵, M.C. Danisch ⁹⁵, A. Danu ⁶⁴, P. Das ⁸¹, P. Das ⁴, S. Das ⁴, A.R. Dash ¹²⁷, S. Dash ⁴⁸, A. De Caro ²⁹, G. de Cataldo ⁵¹, J. de Cuveland³⁹, A. De Falco ²³, D. De Gruttola ²⁹, N. De Marco ⁵⁷, C. De Martin ²⁴, S. De Pasquale ²⁹, R. Deb ¹³⁵, R. Del Grande ⁹⁶, L. Dello Stritto ²⁹, W. Deng ⁶, P. Dhankher ¹⁹, D. Di Bari ³², A. Di Mauro ³³, B. Diab ¹³¹, R.A. Diaz ^{143,7}, T. Dietel ¹¹⁵, Y. Ding ⁶, R. Divià ³³, D.U. Dixit ¹⁹, Ø. Djuvsland²¹, U. Dmitrieva ¹⁴², A. Dobrin ⁶⁴, B. Dönigus ⁶⁵, J.M. Dubinski ¹³⁷, A. Dubla ⁹⁸, S. Dudi ⁹¹, P. Dupieux ¹²⁸, M. Durkac¹⁰⁷, N. Dzalaiova¹³, T.M. Eder ¹²⁷, R.J. Ehlers ⁷⁵, F. Eisenhut ⁶⁵, R. Ejima⁹³, D. Elia ⁵¹, B. Erazmus ¹⁰¹, F. Ercolessi ²⁶, F. Erhardt ⁹⁰, M.R. Ersdal²¹, B. Espagnon ¹³², G. Eulisse ³³, D. Evans ¹⁰¹, S. Evdokimov ¹⁴², L. Fabbietti ⁹⁶, M. Faggin ²⁸, J. Faivre ⁷⁴, F. Fan ⁶, W. Fan ⁷⁵, A. Fantoni ⁵⁰, M. Fasel ⁸⁸, P. Fecchio³⁰, A. Feliciello ⁵⁷, G. Feofilov ¹⁴², A. Fernández Téllez ⁴⁵, L. Ferrandi ¹¹¹, M.B. Ferrer ³³, A. Ferrero ¹³¹, C. Ferrero ⁵⁷, A. Ferretti ²⁵, V.J.G. Feuillard ⁹⁵, V. Filova ³⁶, D. Finogeev ¹⁴², F.M. Fionda ⁵³, F. Flor ¹¹⁷, A.N. Flores ¹⁰⁹, S. Foertsch ⁶⁹, I. Fokin ⁹⁵, S. Fokin ¹⁴², E. Fragiaco ⁵⁸, E. Frajna ⁴⁷, U. Fuchs ³³, N. Funicello ²⁹, C. Furget ⁷⁴, A. Furs ¹⁴², T. Fusayasu ⁹⁹, J.J. Gaardhøje ⁸⁴, M. Gagliardi ²⁵, A.M. Gago ¹⁰², T. Gahlaut⁴⁸, C.D. Galvan ¹¹⁰, D.R. Gangadharan ¹¹⁷, P. Ganoti ⁷⁹, C. Garabatos ⁹⁸, T. García Chávez ⁴⁵, E. García-Solis ⁹, C. Gargiulo ³³, K. Garner¹²⁷, P. Gasik ⁹⁸, A. Gautam ¹¹⁹, M.B. Gay Ducati ⁶⁷, M. Germain ¹⁰⁴, A. Ghimouz¹²⁶, C. Ghosh¹³⁶, M. Giacalone ⁵², G. Gioachin ³⁰, P. Giubellino ^{98,57}, P. Giubiliato ²⁸, A.M.C. Glaenger ¹³¹, P. Glässel ⁹⁵, E. Glimos ¹²³, D.J.Q. Goh⁷⁷, V. Gonzalez ¹³⁸, M. Gorgon ², K. Goswami ⁴⁹, S. Gotovac³⁴, V. Grabski ⁶⁸, L.K. Graczykowski ¹³⁷, E. Grecka ⁸⁷, A. Grelli ⁶⁰, C. Grigoras ³³, V. Grigoriev ¹⁴², S. Grigoryan ^{143,1}, F. Grosa ³³, J.F. Grosse-Oetringhaus ³³, R. Grosso ⁹⁸, D. Grund ³⁶, G.G. Guardiano ¹¹², R. Guernane ⁷⁴, M. Guilbaud ¹⁰⁴, K. Gulbrandsen ⁸⁴, T. Gündem ⁶⁵, T. Gunji ¹²⁵, W. Guo ⁶,

A. Gupta ⁹², R. Gupta ⁹², R. Gupta ⁴⁹, K. Gwizdziel ¹³⁷, L. Gyulai ⁴⁷, C. Hadjidakis ¹³², F.U. Haider ⁹², H. Hamagaki ⁷⁷, A. Hamdi ⁷⁵, Y. Han ¹⁴⁰, B.G. Hanley ¹³⁸, R. Hannigan ¹⁰⁹, J. Hansen ⁷⁶, M.R. Haque ¹³⁷, J.W. Harris ¹³⁹, A. Harton ⁹, H. Hassan ⁸⁸, D. Hatzifotiadou ⁵², P. Hauer ⁴³, L.B. Havener ¹³⁹, S.T. Heckel ⁹⁶, E. Hellbär ⁹⁸, H. Helstrup ³⁵, M. Hemmer ⁶⁵, T. Herman ³⁶, G. Herrera Corral ⁸, F. Herrmann ¹²⁷, S. Herrmann ¹²⁹, K.F. Hetland ³⁵, B. Heybeck ⁶⁵, H. Hillemanns ³³, B. Hippolyte ¹³⁰, F.W. Hoffmann ⁷¹, B. Hofman ⁶⁰, G.H. Hong ¹⁴⁰, M. Horst ⁹⁶, A. Horzyk ², Y. Hou ⁶, P. Hristov ³³, C. Hughes ¹²³, P. Huhn ⁶⁵, L.M. Huhta ¹¹⁸, T.J. Humanic ⁸⁹, A. Hutson ¹¹⁷, D. Hutter ³⁹, R. Ilkaev ¹⁴², H. Ilyas ¹⁴, M. Inaba ¹²⁶, G.M. Innocenti ³³, M. Ippolitov ¹⁴², A. Isakov ^{85,87}, T. Isidori ¹¹⁹, M.S. Islam ¹⁰⁰, M. Ivanov ¹³, M. Ivanov ⁹⁸, V. Ivanov ¹⁴², K.E. Iversen ⁷⁶, M. Jablonski ², B. Jacak ⁷⁵, N. Jacazio ²⁶, P.M. Jacobs ⁷⁵, S. Jadlovská ¹⁰⁷, J. Jadlovsky ¹⁰⁷, S. Jaelani ⁸³, C. Jahnke ¹¹², M.J. Jakubowska ¹³⁷, M.A. Janik ¹³⁷, T. Janson ⁷¹, S. Ji ¹⁷, S. Jia ¹⁰, A.A.P. Jimenez ⁶⁶, F. Jonas ^{88,127}, D.M. Jones ¹²⁰, J.M. Jowett ^{33,98}, J. Jung ⁶⁵, M. Jung ⁶⁵, A. Junique ³³, A. Jusko ¹⁰¹, M.J. Kabus ^{33,137}, J. Kaewjai ¹⁰⁶, P. Kalinak ⁶¹, A.S. Kalteyer ⁹⁸, A. Kalweit ³³, V. Kaplin ¹⁴², A. Karasu Uysal ⁷³, D. Karatovic ⁹⁰, O. Karavichev ¹⁴², T. Karavicheva ¹⁴², P. Karczmarczyk ¹³⁷, E. Karpechev ¹⁴², U. Kebschull ⁷¹, R. Keidel ¹⁴¹, D.L.D. Keijdener ⁶⁰, M. Keil ³³, B. Ketzer ⁴³, S.S. Khade ⁴⁹, A.M. Khan ^{121,6}, S. Khan ¹⁶, A. Khanzadeev ¹⁴², Y. Kharlov ¹⁴², A. Khatun ¹¹⁹, A. Khuntia ³⁶, B. Kileng ³⁵, B. Kim ¹⁰⁵, C. Kim ¹⁷, D.J. Kim ¹¹⁸, E.J. Kim ⁷⁰, J. Kim ¹⁴⁰, J.S. Kim ⁴¹, J. Kim ⁵⁹, J. Kim ⁷⁰, M. Kim ¹⁹, S. Kim ¹⁸, T. Kim ¹⁴⁰, K. Kimura ⁹³, S. Kirsch ⁶⁵, I. Kisel ³⁹, S. Kiselev ¹⁴², A. Kisiel ¹³⁷, J.P. Kitowski ², J.L. Klay ⁵, J. Klein ³³, S. Klein ⁷⁵, C. Klein-Bösing ¹²⁷, M. Kleiner ⁶⁵, T. Klemenz ⁹⁶, A. Kluge ³³, A.G. Knospe ¹¹⁷, C. Kobdaj ¹⁰⁶, T. Kollegger ⁹⁸, A. Kondratyev ¹⁴³, N. Kondratyeva ¹⁴², E. Kondratyuk ¹⁴², J. König ⁶⁵, S.A. Königstorfer ⁹⁶, P.J. Konopka ³³, G. Kornakov ¹³⁷, M. Korwieser ⁹⁶, S.D. Koryciak ², A. Kotliarov ⁸⁷, V. Kovalenko ¹⁴², M. Kowalski ¹⁰⁸, V. Kozuharov ³⁷, I. Králik ⁶¹, A. Kravčáková ³⁸, L. Krcal ^{33,39}, M. Krivda ^{101,61}, F. Krizek ⁸⁷, K. Krizkova Gajdosova ³³, M. Kroesen ⁹⁵, M. Krüger ⁶⁵, D.M. Krupova ³⁶, E. Kryshen ¹⁴², V. Kučera ⁵⁹, C. Kuhn ¹³⁰, P.G. Kuijer ⁸⁵, T. Kumaoka ¹²⁶, D. Kumar ¹³⁶, L. Kumar ⁹¹, N. Kumar ⁹¹, S. Kumar ³², S. Kundu ³³, P. Kurashvili ⁸⁰, A. Kurepin ¹⁴², A.B. Kurepin ¹⁴², A. Kuryakin ¹⁴², S. Kushpil ⁸⁷, M.J. Kweon ⁵⁹, Y. Kwon ¹⁴⁰, S.L. La Pointe ³⁹, P. La Rocca ²⁷, A. Lakrathok ¹⁰⁶, M. Lamanna ³³, A.R. Landou ^{74,116}, R. Langoy ¹²², P. Larionov ³³, E. Laudi ³³, L. Lautner ^{33,96}, R. Lavicka ¹⁰³, R. Lea ^{135,56}, H. Lee ¹⁰⁵, I. Legrand ⁴⁶, G. Le Gras ¹²⁷, J. Lehrbach ³⁹, T.M. Lelek ², R.C. Lemmon ⁸⁶, I. León Monzón ¹¹⁰, M.M. Lesch ⁹⁶, E.D. Lesser ¹⁹, P. Lévai ⁴⁷, X. Li ¹⁰, X.L. Li ⁶, J. Lien ¹²², R. Lietava ¹⁰¹, I. Likmeta ¹¹⁷, B. Lim ²⁵, S.H. Lim ¹⁷, V. Lindenstruth ³⁹, A. Lindner ⁴⁶, C. Lippmann ⁹⁸, A. Liu ¹⁹, D.H. Liu ⁶, J. Liu ¹²⁰, G.S.S. Liveraro ¹¹², I.M. Lofnes ²¹, C. Loizides ⁸⁸, S. Lokos ¹⁰⁸, J. Lömker ⁶⁰, P. Loncar ³⁴, X. Lopez ¹²⁸, E. López Torres ⁷, P. Lu ^{98,121}, J.R. Luhder ¹²⁷, M. Lunardon ²⁸, G. Luparello ⁵⁸, Y.G. Ma ⁴⁰, M. Mager ³³, A. Maire ¹³⁰, E.M. Majerz ², M.V. Makariev ³⁷, M. Malaev ¹⁴², G. Malfattore ²⁶, N.M. Malik ⁹², Q.W. Malik ²⁰, S.K. Malik ⁹², L. Malinina ^{1, VII, 143}, D. Mallick ^{132,81}, N. Mallick ⁴⁹, G. Mandaglio ^{31,54}, S.K. Mandal ⁸⁰, V. Manko ¹⁴², F. Manso ¹²⁸, V. Manzari ⁵¹, Y. Mao ⁶, R.W. Marcjan ², G.V. Margagliotti ²⁴, A. Margotti ⁵², A. Marín ⁹⁸, C. Markert ¹⁰⁹, P. Martinengo ³³, M.I. Martínez ⁴⁵, G. Martínez García ¹⁰⁴, M.P.P. Martins ¹¹¹, S. Masciocchi ⁹⁸, M. Masera ²⁵, A. Masoni ⁵³, L. Massacrier ¹³², O. Massen ⁶⁰, A. Mastroserio ^{133,51}, O. Matonoha ⁷⁶, S. Mattiazzo ²⁸, P.F.T. Matuoka ¹¹¹, A. Matyja ¹⁰⁸, C. Mayer ¹⁰⁸, A.L. Mazuecos ³³, F. Mazzaschi ²⁵, M. Mazzilli ³³, J.E. Mdhluli ¹²⁴, A.F. Mechler ⁶⁵, Y. Melikyan ⁴⁴, A. Menchaca-Rocha ⁶⁸, E. Meninno ¹⁰³, A.S. Menon ¹¹⁷, M. Meres ¹³, S. Mhlanga ^{115,69}, Y. Miake ¹²⁶, L. Micheletti ³³, L.C. Migliorin ¹²⁹, D.L. Mihaylov ⁹⁶, K. Mikhaylov ^{143,142}, A.N. Mishra ⁴⁷, D. Miśkowiec ⁹⁸, A. Modak ⁴, A.P. Mohanty ⁶⁰, B. Mohanty ⁸¹, M. Mohisin Khan ^{V, 16}, M.A. Molander ⁴⁴, S. Monira ¹³⁷, Z. Moravcova ⁸⁴, C. Mordasini ¹¹⁸, D.A. Moreira De Godoy ¹²⁷, I. Morozov ¹⁴², A. Morsch ³³, T. Mrnjavac ³³, V. Muccifora ⁵⁰, S. Muhuri ¹³⁶, J.D. Mulligan ⁷⁵, A. Mulliri ²³, M.G. Munhoz ¹¹¹, R.H. Munzer ⁶⁵, H. Murakami ¹²⁵, S. Murray ¹¹⁵, L. Musa ³³, J. Musinsky ⁶¹, J.W. Myrcha ¹³⁷, B. Naik ¹²⁴, A.I. Nambrath ¹⁹, B.K. Nandi ⁴⁸, R. Nania ⁵², E. Nappi ⁵¹, A.F. Nassirpour ^{18,76}, A. Nath ⁹⁵, C. Nattrass ¹²³, M.N. Naydenov ³⁷, A. Neagu ²⁰, A. Negru ¹¹⁴, L. Nellen ⁶⁶, R. Nepeivoda ⁷⁶, S. Nese ²⁰, G. Neskovic ³⁹, N. Nicassio ⁵¹, B.S. Nielsen ⁸⁴, E.G. Nielsen ⁸⁴, S. Nikolaev ¹⁴², S. Nikulin ¹⁴², V. Nikulin ¹⁴², F. Noferini ⁵², S. Noh ¹², P. Nomokonov ¹⁴³, J. Norman ¹²⁰, N. Novitzky ¹²⁶, P. Nowakowski ¹³⁷, A. Nyanin ¹⁴², J. Nystrand ²¹, M. Ogino ⁷⁷, S. Oh ¹⁸, A. Ohlson ⁷⁶, V.A. Okorokov ¹⁴², J. Oleniacz ¹³⁷, A.C. Oliveira Da Silva ¹²³, M.H. Oliver ¹³⁹, A. Onnerstad ¹¹⁸, C. Oppedisano ⁵⁷, A. Ortiz Velasquez ⁶⁶, J. Otwinowski ¹⁰⁸, M. Oya ⁹³, K. Oyama ⁷⁷,

Y. Pachmayer⁹⁵, S. Padhan⁴⁸, D. Pagano^{135,56}, G. Paic⁶⁶, S. Paisano-Guzmán⁴⁵, A. Palasciano⁵¹, S. Panebianco¹³¹, H. Park¹²⁶, H. Park¹⁰⁵, J. Park⁵⁹, J.E. Parkkila³³, Y. Patley⁴⁸, R.N. Patra⁹², B. Paul²³, H. Pei⁶, T. Peitzmann⁶⁰, X. Peng¹¹, M. Pennisi²⁵, S. Perciballi²⁵, D. Peresunko¹⁴², G.M. Perez⁷, Y. Pestov¹⁴², V. Petrov¹⁴², M. Petrovici⁴⁶, R.P. Pezzi^{104,67}, S. Piano⁵⁸, M. Pikna¹³, P. Pillot¹⁰⁴, O. Pinazza^{52,33}, L. Pinsky¹¹⁷, C. Pinto⁹⁶, S. Pisano⁵⁰, M. Płoskoń⁷⁵, M. Planinic⁹⁰, F. Pliquet⁶⁵, M.G. Poghosyan⁸⁸, B. Polichtchouk¹⁴², S. Politano³⁰, N. Poljak⁹⁰, A. Pop⁴⁶, S. Porteboeuf-Houssais¹²⁸, V. Pozdniakov¹⁴³, I.Y. Pozos⁴⁵, K.K. Pradhan⁴⁹, S.K. Prasad⁴, S. Prasad⁴⁹, R. Preghenella⁵², F. Prino⁵⁷, C.A. Pruneau¹³⁸, I. Pshenichnov¹⁴², M. Puccio³³, S. Pucillo²⁵, Z. Pugelova¹⁰⁷, S. Qiu⁸⁵, L. Quaglia²⁵, R.E. Quishpe¹¹⁷, S. Ragoni¹⁵, A. Rai¹³⁹, A. Rakotozafindrabe¹³¹, L. Ramello^{134,57}, F. Rami¹³⁰, T.A. Rancien⁷⁴, M. Rasa²⁷, S.S. Räsänen⁴⁴, R. Rath⁵², M.P. Rauch²¹, I. Ravasenga⁸⁵, K.F. Read^{88,123}, C. Reckziegel¹¹³, A.R. Redelbach³⁹, K. Redlich^{VI,80}, C.A. Retz⁹⁸, H.D. Regules-Medel⁴⁵, A. Rehman²¹, F. Reidt³³, H.A. Reme-Ness³⁵, Z. Rescakova³⁸, K. Reyers⁹⁵, A. Riabov¹⁴², V. Riabov¹⁴², R. Ricci²⁹, M. Richter²⁰, A.A. Riedel⁹⁶, W. Riegler³³, A.G. Riffero²⁵, C. Ristea⁶⁴, M.V. Rodriguez³³, M. Rodríguez Cahuanti⁴⁵, S.A. Rodríguez Ramírez⁴⁵, K. Røed²⁰, R. Rogalev¹⁴², E. Rogochaya¹⁴³, T.S. Rogoschinski⁶⁵, D. Rohr³³, D. Röhrich²¹, P.F. Rojas⁴⁵, S. Rojas Torres³⁶, P.S. Rokita¹³⁷, G. Romanenko²⁶, F. Ronchetti⁵⁰, A. Rosano^{31,54}, E.D. Rosas⁶⁶, K. Roslon¹³⁷, A. Rossi⁵⁵, A. Roy⁴⁹, S. Roy⁴⁸, N. Rubini²⁶, D. Ruggiano¹³⁷, R. Rui²⁴, P.G. Russek², R. Russo⁸⁵, A. Rustamov⁸², E. Ryabinkin¹⁴², Y. Ryabov¹⁴², A. Rybicki¹⁰⁸, H. Rytkonen¹¹⁸, J. Ryu¹⁷, W. Rzeska¹³⁷, O.A.M. Saarimäki⁴⁴, S. Sadhu³², S. Sadovsky¹⁴², J. Saetre²¹, K. Šafařík³⁶, P. Saha⁴², S.K. Saha⁴, S. Saha⁸¹, B. Sahoo⁴⁸, B. Sahoo⁴⁹, R. Sahoo⁴⁹, S. Sahoo⁶², D. Sahu⁴⁹, P.K. Sahu⁶², J. Saini¹³⁶, K. Sajdakova³⁸, S. Sakai¹²⁶, M.P. Salvan⁹⁸, S. Sambyal⁹², D. Samitz¹⁰³, I. Sanna^{33,96}, T.B. Saramela¹¹¹, P. Sarma⁴², V. Sarritzu²³, V.M. Sarti⁹⁶, M.H.P. Sas¹³⁹, J. Schambach⁸⁸, H.S. Scheid⁶⁵, C. Schiava⁴⁶, R. Schicker⁹⁵, A. Schmah⁹⁸, C. Schmidt⁹⁸, H.R. Schmidt⁹⁴, M.O. Schmidt³³, M. Schmidt⁹⁴, N.V. Schmidt⁸⁸, A.R. Schmier¹²³, R. Schotter¹³⁰, A. Schröter³⁹, J. Schukraft³³, K. Schweda⁹⁸, G. Scioli²⁶, E. Scomarini⁵⁷, J.E. Seger¹⁵, Y. Sekiguchi¹²⁵, D. Sekihata¹²⁵, M. Selina⁸⁵, I. Selyuzhenkov⁹⁸, S. Senyukov¹³⁰, J.J. Seo^{95,59}, D. Serebryakov¹⁴², L. Šerkšnytė⁹⁶, A. Sevcenco⁶⁴, T.J. Shaba⁶⁹, A. Shabetai¹⁰⁴, R. Shahoyan³³, A. Shangaraev¹⁴², A. Sharma⁹¹, B. Sharma⁹², D. Sharma⁴⁸, H. Sharma^{55,108}, M. Sharma⁹², S. Sharma⁷⁷, S. Sharma⁹², U. Sharma⁹², A. Shatat¹³², O. Sheibani¹¹⁷, K. Shigaki⁹³, M. Shimomura⁷⁸, J. Shin¹², S. Shirinkin¹⁴², Q. Shou⁴⁰, Y. Sibiriak¹⁴², S. Siddhanta⁵³, T. Siemiarczuk⁸⁰, T.F. Silva¹¹¹, D. Silvermyr⁷⁶, T. Simantathammakul¹⁰⁶, R. Simeonov³⁷, B. Singh⁹², B. Singh⁹⁶, K. Singh⁴⁹, R. Singh⁸¹, R. Singh⁹², R. Singh⁴⁹, S. Singh¹⁶, V.K. Singh¹³⁶, V. Singhal¹³⁶, T. Sinha¹⁰⁰, B. Sitar¹³, M. Sitta^{134,57}, T.B. Skaali²⁰, G. Skorodumovs⁹⁵, M. Slupecki⁴⁴, N. Smirnov¹³⁹, R.J.M. Snellings⁶⁰, E.H. Solheim²⁰, J. Song¹¹⁷, A. Songmoonak¹⁰⁶, C. Sonnabend^{33,98}, F. Soramel²⁸, A.B. Soto-herandez⁸⁹, R. Spijkers⁸⁵, I. Sputowska¹⁰⁸, J. Staa⁷⁶, J. Stachel⁹⁵, I. Stan⁶⁴, P.J. Steffanic¹²³, S.F. Stiefelmaier⁹⁵, D. Stocco¹⁰⁴, I. Storehaug²⁰, P. Stratmann¹²⁷, S. Strazzi²⁶, A. Sturniolo^{31,54}, C.P. Stylianidis⁸⁵, A.A.P. Suaide¹¹¹, C. Suire¹³², M. Sukhanov¹⁴², M. Suljic³³, R. Sultanov¹⁴², V. Sumberia⁹², S. Sumowidagdo⁸³, S. Swain⁶², I. Szarka¹³, M. Szymkowski¹³⁷, S.F. Taghavi⁹⁶, G. Taillepied⁹⁸, J. Takahashi¹¹², G.J. Tambave⁸¹, S. Tang⁶, Z. Tang¹²¹, J.D. Tapia Takaki¹¹⁹, N. Tapus¹¹⁴, L.A. Tarasovicova¹²⁷, M.G. Tazila⁴⁶, G.F. Tassielli³², A. Tauro³³, A. Tavira García¹³², G. Tejeda Muñoz⁴⁵, A. Telesca³³, L. Terlizzi²⁵, C. Terrevoli¹¹⁷, S. Thakur⁴, D. Thomas¹⁰⁹, A. Tikhonov¹⁴², A.R. Timmins¹¹⁷, M. Tkacik¹⁰⁷, T. Tkacik¹⁰⁷, A. Toia⁶⁵, R. Tokumoto⁹³, K. Tomohiro⁹³, N. Topilskaya¹⁴², M. Toppi⁵⁰, T. Tork¹³², V.V. Torres¹⁰⁴, A.G. Torres Ramos³², A. Trifiró^{31,54}, A.S. Triolo^{33,31,54}, S. Tripathy⁵², T. Tripathy⁴⁸, S. Trogolo³³, V. Trubnikov³, W.H. Trzaska¹¹⁸, T.P. Trzcinski¹³⁷, A. Tumkin¹⁴², R. Turrisi⁵⁵, T.S. Tveter²⁰, K. Ullaland²¹, B. Ulukutlu⁹⁶, A. Uras¹²⁹, G.L. Usai²³, M. Vala³⁸, N. Valle²², L.V.R. van Doremalen⁶⁰, M. van Leeuwen⁸⁵, C.A. van Veen⁹⁵, R.J.G. van Weelden⁸⁵, P. Vande Vyvre³³, D. Varga⁴⁷, Z. Varga⁴⁷, M. Vasileiou⁷⁹, A. Vasiliev¹⁴², O. Vázquez Doce⁵⁰, O. Vazquez Rueda¹¹⁷, V. Vechemin¹⁴², E. Vercellin²⁵, S. Vergara Limón⁴⁵, R. Verma⁴⁸, L. Vermunt⁹⁸, R. Vértesi⁴⁷, M. Verweij⁶⁰, L. Vickovic³⁴, Z. Vilakazi¹²⁴, O. Villalobos Baillie¹⁰¹, A. Villani²⁴, G. Vito⁵¹, A. Vinogradov¹⁴², T. Virgili²⁹, M.M.O. Virta¹¹⁸, V. Vislavicius⁷⁶, A. Vodopyanov¹⁴³, B. Volkel³³, M.A. Völkl⁹⁵, K. Voloshin¹⁴², S.A. Voloshin¹³⁸, G. Volpe³², B. von Haller³³, I. Vorobyev⁹⁶, N. Vozniuk¹⁴², J. Vrláková³⁸, J. Wan⁴⁰, C. Wang⁴⁰, D. Wang⁴⁰, Y. Wang⁴⁰, Y. Wang⁶, A. Wegrzynek³³, F.T. Weiglhofer³⁹, S.C. Wenzel³³, J.P. Wessels¹²⁷, J. Wiechula⁶⁵, J. Wikne²⁰, G. Wilk⁸⁰, J. Wilkinson⁹⁸, G.A. Willems¹²⁷, B. Windelband⁹⁵, M. Winn¹³¹, J.R. Wright¹⁰⁹,

W. Wu⁴⁰, Y. Wu¹²¹, R. Xu⁶, A. Yadav⁴³, A.K. Yadav¹³⁶, S. Yalcin⁷³, Y. Yamaguchi⁹³, S. Yang²¹, S. Yano⁹³, Z. Yin⁶, I.-K. Yoo¹⁷, J.H. Yoon⁵⁹, H. Yu¹², S. Yuan²¹, A. Yuncu⁹⁵, V. Zaccolo²⁴, C. Zampolli³³, F. Zanone⁹⁵, N. Zardoshti³³, A. Zarochentsev¹⁴², P. Závada⁶³, N. Zaviyalov¹⁴², M. Zhalov¹⁴², B. Zhang⁶, C. Zhang¹³¹, L. Zhang⁴⁰, S. Zhang⁴⁰, X. Zhang⁶, Y. Zhang¹²¹, Z. Zhang⁶, M. Zhao¹⁰, V. Zherebchevskii¹⁴², Y. Zhi¹⁰, D. Zhou⁶, Y. Zhou⁸⁴, J. Zhu^{55,6}, Y. Zhu⁶, S.C. Zugarvel⁵⁷, N. Zurlo^{135,56}

Affiliation Notes

^I Deceased

^{II} Also at: Max-Planck-Institut für Physik, Munich, Germany

^{III} Also at: Italian National Agency for New Technologies, Energy and Sustainable Economic Development (ENEA), Bologna, Italy

^{IV} Also at: Dipartimento DET del Politecnico di Torino, Turin, Italy

^V Also at: Department of Applied Physics, Aligarh Muslim University, Aligarh, India

^{VI} Also at: Institute of Theoretical Physics, University of Wrocław, Poland

^{VII} Also at: An institution covered by a cooperation agreement with CERN

Collaboration Institutes

¹ A.I. Alikhanyan National Science Laboratory (Yerevan Physics Institute) Foundation, Yerevan, Armenia

² AGH University of Krakow, Cracow, Poland

³ Bogolyubov Institute for Theoretical Physics, National Academy of Sciences of Ukraine, Kiev, Ukraine

⁴ Bose Institute, Department of Physics and Centre for Astroparticle Physics and Space Science (CAPSS), Kolkata, India

⁵ California Polytechnic State University, San Luis Obispo, California, United States

⁶ Central China Normal University, Wuhan, China

⁷ Centro de Aplicaciones Tecnológicas y Desarrollo Nuclear (CEADEN), Havana, Cuba

⁸ Centro de Investigación y de Estudios Avanzados (CINVESTAV), Mexico City and Mérida, Mexico

⁹ Chicago State University, Chicago, Illinois, United States

¹⁰ China Institute of Atomic Energy, Beijing, China

¹¹ China University of Geosciences, Wuhan, China

¹² Chungbuk National University, Cheongju, Republic of Korea

¹³ Comenius University Bratislava, Faculty of Mathematics, Physics and Informatics, Bratislava, Slovak Republic

¹⁴ COMSATS University Islamabad, Islamabad, Pakistan

¹⁵ Creighton University, Omaha, Nebraska, United States

¹⁶ Department of Physics, Aligarh Muslim University, Aligarh, India

¹⁷ Department of Physics, Pusan National University, Pusan, Republic of Korea

¹⁸ Department of Physics, Sejong University, Seoul, Republic of Korea

¹⁹ Department of Physics, University of California, Berkeley, California, United States

²⁰ Department of Physics, University of Oslo, Oslo, Norway

²¹ Department of Physics and Technology, University of Bergen, Bergen, Norway

²² Dipartimento di Fisica, Università di Pavia, Pavia, Italy

²³ Dipartimento di Fisica dell'Università and Sezione INFN, Cagliari, Italy

²⁴ Dipartimento di Fisica dell'Università and Sezione INFN, Trieste, Italy

²⁵ Dipartimento di Fisica dell'Università and Sezione INFN, Turin, Italy

²⁶ Dipartimento di Fisica e Astronomia dell'Università and Sezione INFN, Bologna, Italy

²⁷ Dipartimento di Fisica e Astronomia dell'Università and Sezione INFN, Catania, Italy

²⁸ Dipartimento di Fisica e Astronomia dell'Università and Sezione INFN, Padova, Italy

²⁹ Dipartimento di Fisica 'E.R. Caianiello' dell'Università and Gruppo Collegato INFN, Salerno, Italy

³⁰ Dipartimento DISAT del Politecnico and Sezione INFN, Turin, Italy

³¹ Dipartimento di Scienze MIIFT, Università di Messina, Messina, Italy

³² Dipartimento Interateneo di Fisica 'M. Merlin' and Sezione INFN, Bari, Italy

³³ European Organization for Nuclear Research (CERN), Geneva, Switzerland

³⁴ Faculty of Electrical Engineering, Mechanical Engineering and Naval Architecture, University of Split, Split, Croatia

- ³⁵ Faculty of Engineering and Science, Western Norway University of Applied Sciences, Bergen, Norway
- ³⁶ Faculty of Nuclear Sciences and Physical Engineering, Czech Technical University in Prague, Prague, Czech Republic
- ³⁷ Faculty of Physics, Sofia University, Sofia, Bulgaria
- ³⁸ Faculty of Science, P.J. Šafárik University, Košice, Slovak Republic
- ³⁹ Frankfurt Institute for Advanced Studies, Johann Wolfgang Goethe-Universität Frankfurt, Frankfurt, Germany
- ⁴⁰ Fudan University, Shanghai, China
- ⁴¹ Gangneung-Wonju National University, Gangneung, Republic of Korea
- ⁴² Gauhati University, Department of Physics, Guwahati, India
- ⁴³ Helmholtz-Institut für Strahlen- und Kernphysik, Rheinische Friedrich-Wilhelms-Universität Bonn, Bonn, Germany
- ⁴⁴ Helsinki Institute of Physics (HIP), Helsinki, Finland
- ⁴⁵ High Energy Physics Group, Universidad Autónoma de Puebla, Puebla, Mexico
- ⁴⁶ Horia Hulubei National Institute of Physics and Nuclear Engineering, Bucharest, Romania
- ⁴⁷ HUN-REN Wigner Research Centre for Physics, Budapest, Hungary
- ⁴⁸ Indian Institute of Technology Bombay (IIT), Mumbai, India
- ⁴⁹ Indian Institute of Technology Indore, Indore, India
- ⁵⁰ INFN, Laboratori Nazionali di Frascati, Frascati, Italy
- ⁵¹ INFN, Sezione di Bari, Bari, Italy
- ⁵² INFN, Sezione di Bologna, Bologna, Italy
- ⁵³ INFN, Sezione di Cagliari, Cagliari, Italy
- ⁵⁴ INFN, Sezione di Catania, Catania, Italy
- ⁵⁵ INFN, Sezione di Padova, Padova, Italy
- ⁵⁶ INFN, Sezione di Pavia, Pavia, Italy
- ⁵⁷ INFN, Sezione di Torino, Turin, Italy
- ⁵⁸ INFN, Sezione di Trieste, Trieste, Italy
- ⁵⁹ Inha University, Incheon, Republic of Korea
- ⁶⁰ Institute for Gravitational and Subatomic Physics (GRASP), Utrecht University/Nikhef, Utrecht, Netherlands
- ⁶¹ Institute of Experimental Physics, Slovak Academy of Sciences, Košice, Slovak Republic
- ⁶² Institute of Physics, Homi Bhabha National Institute, Bhubaneswar, India
- ⁶³ Institute of Physics of the Czech Academy of Sciences, Prague, Czech Republic
- ⁶⁴ Institute of Space Science (ISS), Bucharest, Romania
- ⁶⁵ Institut für Kernphysik, Johann Wolfgang Goethe-Universität Frankfurt, Frankfurt, Germany
- ⁶⁶ Instituto de Ciencias Nucleares, Universidad Nacional Autónoma de México, Mexico City, Mexico
- ⁶⁷ Instituto de Física, Universidade Federal do Rio Grande do Sul (UFRGS), Porto Alegre, Brazil
- ⁶⁸ Instituto de Física, Universidad Nacional Autónoma de México, Mexico City, Mexico
- ⁶⁹ iThemba LABS, National Research Foundation, Somerset West, South Africa
- ⁷⁰ Jeonbuk National University, Jeonju, Republic of Korea
- ⁷¹ Johann-Wolfgang-Goethe Universität Frankfurt Institut für Informatik, Fachbereich Informatik und Mathematik, Frankfurt, Germany
- ⁷² Korea Institute of Science and Technology Information, Daejeon, Republic of Korea
- ⁷³ KTO Karatay University, Konya, Turkey
- ⁷⁴ Laboratoire de Physique Subatomique et de Cosmologie, Université Grenoble-Alpes, CNRS-IN2P3, Grenoble, France
- ⁷⁵ Lawrence Berkeley National Laboratory, Berkeley, California, United States
- ⁷⁶ Lund University Department of Physics, Division of Particle Physics, Lund, Sweden
- ⁷⁷ Nagasaki Institute of Applied Science, Nagasaki, Japan
- ⁷⁸ Nara Women's University (NWU), Nara, Japan
- ⁷⁹ National and Kapodistrian University of Athens, School of Science, Department of Physics, Athens, Greece
- ⁸⁰ National Centre for Nuclear Research, Warsaw, Poland
- ⁸¹ National Institute of Science Education and Research, Homi Bhabha National Institute, Jatni, India
- ⁸² National Nuclear Research Center, Baku, Azerbaijan
- ⁸³ National Research and Innovation Agency - BRIN, Jakarta, Indonesia
- ⁸⁴ Niels Bohr Institute, University of Copenhagen, Copenhagen, Denmark
- ⁸⁵ Nikhef, National institute for subatomic physics, Amsterdam, Netherlands
- ⁸⁶ Nuclear Physics Group, STFC Daresbury Laboratory, Daresbury, United Kingdom

- ⁸⁷ Nuclear Physics Institute of the Czech Academy of Sciences, Husinec-Řež, Czech Republic
- ⁸⁸ Oak Ridge National Laboratory, Oak Ridge, Tennessee, United States
- ⁸⁹ Ohio State University, Columbus, Ohio, United States
- ⁹⁰ Physics department, Faculty of science, University of Zagreb, Zagreb, Croatia
- ⁹¹ Physics Department, Panjab University, Chandigarh, India
- ⁹² Physics Department, University of Jammu, Jammu, India
- ⁹³ Physics Program and International Institute for Sustainability with Knotted Chiral Meta Matter (SKCM2), Hiroshima University, Hiroshima, Japan
- ⁹⁴ Physikalisches Institut, Eberhard-Karls-Universität Tübingen, Tübingen, Germany
- ⁹⁵ Physikalisches Institut, Ruprecht-Karls-Universität Heidelberg, Heidelberg, Germany
- ⁹⁶ Physik Department, Technische Universität München, Munich, Germany
- ⁹⁷ Politecnico di Bari and Sezione INFN, Bari, Italy
- ⁹⁸ Research Division and ExtreMe Matter Institute EMMI, GSI Helmholtzzentrum für Schwerionenforschung GmbH, Darmstadt, Germany
- ⁹⁹ Saga University, Saga, Japan
- ¹⁰⁰ Saha Institute of Nuclear Physics, Homi Bhabha National Institute, Kolkata, India
- ¹⁰¹ School of Physics and Astronomy, University of Birmingham, Birmingham, United Kingdom
- ¹⁰² Sección Física, Departamento de Ciencias, Pontificia Universidad Católica del Perú, Lima, Peru
- ¹⁰³ Stefan Meyer Institut für Subatomare Physik (SMI), Vienna, Austria
- ¹⁰⁴ SUBATECH, IMT Atlantique, Nantes Université, CNRS-IN2P3, Nantes, France
- ¹⁰⁵ Sungkyunkwan University, Suwon City, Republic of Korea
- ¹⁰⁶ Suranaree University of Technology, Nakhon Ratchasima, Thailand
- ¹⁰⁷ Technical University of Košice, Košice, Slovak Republic
- ¹⁰⁸ The Henryk Niewodniczanski Institute of Nuclear Physics, Polish Academy of Sciences, Cracow, Poland
- ¹⁰⁹ The University of Texas at Austin, Austin, Texas, United States
- ¹¹⁰ Universidad Autónoma de Sinaloa, Culiacán, Mexico
- ¹¹¹ Universidade de São Paulo (USP), São Paulo, Brazil
- ¹¹² Universidade Estadual de Campinas (UNICAMP), Campinas, Brazil
- ¹¹³ Universidade Federal do ABC, Santo Andre, Brazil
- ¹¹⁴ Universitatea Nationala de Stiinta si Tehnologie Politehnica Bucuresti, Bucharest, Romania
- ¹¹⁵ University of Cape Town, Cape Town, South Africa
- ¹¹⁶ University of Derby, Derby, United Kingdom
- ¹¹⁷ University of Houston, Houston, Texas, United States
- ¹¹⁸ University of Jyväskylä, Jyväskylä, Finland
- ¹¹⁹ University of Kansas, Lawrence, Kansas, United States
- ¹²⁰ University of Liverpool, Liverpool, United Kingdom
- ¹²¹ University of Science and Technology of China, Hefei, China
- ¹²² University of South-Eastern Norway, Kongsberg, Norway
- ¹²³ University of Tennessee, Knoxville, Tennessee, United States
- ¹²⁴ University of the Witwatersrand, Johannesburg, South Africa
- ¹²⁵ University of Tokyo, Tokyo, Japan
- ¹²⁶ University of Tsukuba, Tsukuba, Japan
- ¹²⁷ Universität Münster, Institut für Kernphysik, Münster, Germany
- ¹²⁸ Université Clermont Auvergne, CNRS/IN2P3, LPC, Clermont-Ferrand, France
- ¹²⁹ Université de Lyon, CNRS/IN2P3, Institut de Physique des 2 Infinis de Lyon, Lyon, France
- ¹³⁰ Université de Strasbourg, CNRS, IPHC UMR 7178, F-67000 Strasbourg, France, Strasbourg, France
- ¹³¹ Université Paris-Saclay, Centre d’Etudes de Saclay (CEA), IRFU, Département de Physique Nucléaire (DPhN), Saclay, France
- ¹³² Université Paris-Saclay, CNRS/IN2P3, IJCLab, Orsay, France
- ¹³³ Università degli Studi di Foggia, Foggia, Italy
- ¹³⁴ Università del Piemonte Orientale, Vercelli, Italy
- ¹³⁵ Università di Brescia, Brescia, Italy
- ¹³⁶ Variable Energy Cyclotron Centre, Homi Bhabha National Institute, Kolkata, India
- ¹³⁷ Warsaw University of Technology, Warsaw, Poland
- ¹³⁸ Wayne State University, Detroit, Michigan, United States
- ¹³⁹ Yale University, New Haven, Connecticut, United States

¹⁴⁰ Yonsei University, Seoul, Republic of Korea

¹⁴¹ Zentrum für Technologie und Transfer (ZTT), Worms, Germany

¹⁴² Affiliated with an institute covered by a cooperation agreement with CERN

¹⁴³ Affiliated with an international laboratory covered by a cooperation agreement with CERN.